

# NAVAL POSTGRADUATE SCHOOL

## Monterey, California



### THESIS

#### ANALYTICAL TRANSMISSION ELECTRON MICROSCOPY STUDIES ON COPPER-ALUMINA INTERFACES

by

Richard Y. Hashimoto

June 1999

Advisor:

Alan G. Fox

Approved for public release; distribution is unlimited.

DTIC QUALITY INSPECTED 4

19990510 018

REPORT DOCUMENTATION PAGE			Form Approved OMB No. 0704-0188	
Public reporting burden for this collection of information is estimated to average 1 hour per response, including the time for reviewing instruction, searching existing data sources, gathering and maintaining the data needed, and completing and reviewing the collection of information. Send comments regarding this burden estimate or any other aspect of this collection of information, including suggestions for reducing this burden, to Washington Headquarters Services, Directorate for Information Operations and Reports, 1215 Jefferson Davis Highway, Suite 1204, Arlington, VA 22202-4302, and to the Office of Management and Budget, Paperwork Reduction Project (0704-0188) Washington DC 20503.				
1. AGENCY USE ONLY (Leave blank)		2. REPORT DATE June 1999		3. REPORT TYPE AND DATES COVERED Master's Thesis
4. TITLE AND SUBTITLE ANALYTICAL TRANSMISSION ELECTRON MICROSCOPY STUDIES ON COPPER-ALUMINA INTERFACES			5. FUNDING NUMBERS	
6. AUTHOR(S) Hashimoto, Richard Y.				
7. PERFORMING ORGANIZATION NAME(S) AND ADDRESS(ES) Naval Postgraduate School Monterey CA 93943-5000			8. PERFORMING ORGANIZATION REPORT NUMBER	
9. SPONSORING/MONITORING AGENCY NAME(S) AND ADDRESS(ES)			10. SPONSORING/MONITORING AGENCY REPORT NUMBER	
11. SUPPLEMENTARY NOTES. The views expressed in this thesis are those of the author and do not reflect the official policy or position of the Department of Defense or the U.S. Government.				
12a. DISTRIBUTION/AVAILABILITY STATEMENT Approved for public release; distribution is unlimited.			12b. DISTRIBUTION CODE	
13. ABSTRACT (maximum 200 words) A diffusion bonded copper-alumina interface had been studied using energy dispersive x-ray spectroscopy (EDX) and electron energy loss spectroscopy (EELS). Investigations of polycrystalline alumina showed that silica, a common commercial impurity, was present at the triple junctions in the form of fine mullite crystals in a glassy, silicon rich phase. Silicon was also detected along the alumina grain boundaries near triple junctions. There was no observed diffusion of Cu into alumina or alumina into copper. TEM results indicated no interface phase in the these vacuum formed samples. EDX studies of the interfaces revealed that silicon was present in varying concentrations from 1.0 at.% to 10.0 at.%. Using spatial difference, PEELS at the interface showed two distinct residuals: a coordination similar to an aluminosilicate for silicon rich areas and a coordination similar to a metal to metal coordination for low silicon regions. Comparison of the Si rich interface residual PEELS spectra to that of the alumina triple junction PEELS spectra showed that the interface had atomic environments similar to that of an aluminosilicate, such as mullite. The interface results suggest that Si segregation may contribute to the observed higher strength of the metal-ceramic composite by void filling and modified bond character.				
14. SUBJECT TERMS Copper, Alumina, Interface, EDXS, PEELS, Transmission Electron Microscopy			15. NUMBER OF PAGES	
			16. PRICE CODE	
17. SECURITY CLASSIFICATION OF REPORT Unclassified	18. SECURITY CLASSIFICATION OF THIS PAGE Unclassified	19. SECURITY CLASSIFICATION OF ABSTRACT Unclassified	20. LIMITATION OF ABSTRACT UL	

NSN 7540-01-280-5500

Standard Form 298 (Rev. 2-89)  
Prescribed by ANSI Std. Z39-18 298-102



Approved for public release; distribution is unlimited

**ANALYTICAL TRANSMISSION ELECTRON MICROSCOPY  
STUDIES ON COPPER-ALUMINA INTERFACES**

Richard Y. Hashimoto

B.S., M.S.E., University of California Berkeley, 1990

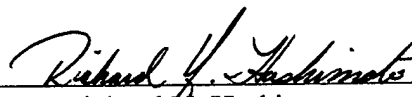
Submitted in partial fulfillment of the  
Requirements for the degree of

**MASTER OF SCIENCE IN ENGINEERING SCIENCE**

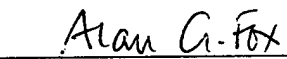
from the


**NAVAL POSTGRADUATE SCHOOL  
June 1999**

Author: \_\_\_\_\_

  
Richard Y. Hashimoto

Approved by: \_\_\_\_\_

  
Alan G. Fox, Thesis Advisor

  
Terry R. McNelley, Chairman  
Department of Mechanical Engineering



## ABSTRACT

A diffusion bonded copper-alumina interface had been studied using energy dispersive x-ray spectroscopy (EDX) and electron energy loss spectroscopy (EELS). Investigations of the bulk alumina (polycrystalline) showed that silica, a common commercial impurity, was present at the triple junctions in the form of fine mullite crystals in a glassy, silicon rich phase. Silicon was also detected along the alumina grain boundaries near triple junctions. There was no observed diffusion of Cu into alumina or alumina into copper. Copper did not appear to be as chemically active at the interface as Al, Si, or O. TEM results indicated no interface phase in the these vacuum formed samples. EDX studies of the interfaces revealed that silicon was present in varying concentrations from 1.0 at.% to 10.0 at.%. Using spatial difference, PEELS at the interface showed two distinct residuals: a coordination similar to an aluminosilicate for silicon rich areas and a coordination similar to a metal to metal coordination for low silicon regions. Comparison of the Si rich interface residual PEELS spectra to that of the alumina triple junction PEELS spectra showed that the interface had atomic environments similar to that of an aluminosilicate, such as mullite. The interface results suggest that Si segregation may contribute to the observed higher strength of the metal-ceramic composite by void filling and modified bond character.



## TABLE OF CONTENTS

I. INTRODUCTION .....	1
II. PREVIOUS WORK.....	7
A.    ALUMINA SUBSTRATE .....	7
B.    COPPER-ALUMINA INTERFACES .....	8
C.    COPPER-ALUMINA MECHANICAL BEHAVIOR.....	10
III. INSTRUMENTATION.....	13
A.    EDXS .....	13
1.    General EDXS.....	13
2.    Sources of error in EDXS .....	15
3.    Spatial resolution in EDXS .....	19
4.    EDXS quantification methods.....	19
B.    PEELS .....	20
1.    General PEELS.....	20
2.    Sources of error in PEELS .....	23
C.    COMPARISON OF DETECTABILITY AND SPATIAL RESOLUTION FOR EDXS AND PEELS .....	24
D.    SPATIAL DIFFERENCE TECHNIQUE.....	25
IV. EXPERIMENTAL .....	27



V. RESULTS AND DISCUSSION .....	29
A.    ALUMINA SUBSTRATE .....	32
1.    Imaging .....	32
2.    EDXS .....	32
3.    PEELS .....	43
4.    Summary of results from alumina substrate .....	54
B.    THE COPPER-ALUMINA INTERFACE .....	57
1.    Imaging .....	57
2.    EDXS .....	57
3.    PEELS .....	60
4.    Summary of results from copper-alumina interface .....	80
VI. CONCLUSIONS.....	83
A.    ALUMINA TRIPLE JUNCTIONS AND GRAIN BOUNDARIES .....	83
B.    COPPER-ALUMINA INTERFACE .....	83
REFERENCES .....	85
INITIAL DISTRIBUTION LIST.....	89

## **ACKNOWLEDGEMENTS**

The author would like to thank Dr Alan Fox, Dr Martin Sanders, Dr Sarath Menon, Dr. Atul Kumar and Dr Nagarajan Rajagopalan for help and useful discussions. In addition, I would like to thank Dr. Rowland Cannon, Dr. Brian Dalgleish, Dr. Toni Tomsia and Dr. Kenji Kaneko for providing the samples and for useful discussions. Finally, I would like to thank my parents, Bob and Kitty Hashimoto, my brother, Ronald Hashimoto, and my great friend Cheslyn Gan for their encouragement and support.



# **I INTRODUCTION**

## **ANALYTICAL TRANSMISSION ELECTRON MICROSCOPY STUDIES OF COPPER-ALUMINA INTERFACES**

As technologies develop there is an increase in demand for new materials. The quest for viable material solutions has increased research and development of traditional metallic, ceramic, semi-conductor, glass, and plastic materials. Unfortunately, the use of a single material often limits the scope in which the material may be applied. This problem has been alleviated by the development of composite systems. A composite system consists of two or more different materials that are combined together to produce a new material. For example, aluminum metal matrix composite (MMC) (an aluminum alloy matrix dispersed with fine ceramic particles) driveshafts are lighter and stiffer than traditional steel alloy equivalents.

Composite systems can have a multitude of material combinations, for example, glass-resin, metal-ceramic, semiconductor-metal, polymer-metal, etc. In particular, metal-ceramic systems have many commercial applications, notably, in the automotive, the aircraft and the aerospace industries. While metal-ceramic systems are seen in many industries, the electronics industry probably has the most applications for metal-ceramic systems. This stems from the fact that many semiconductor devices are composed of layered metal, ceramic, glass and semiconductor materials.

A frequently used metal-ceramic system is the metal-alumina system. Alumina is used as an insulator and/or heat sink for semiconductor and power electronic devices. The use of alumina is precipitated by commercial availability and low cost compared to other

ceramics, such as aluminum nitride. There are many metals that have been used in association with alumina, such as, copper, aluminum, chromium, silver, and gold. In particular, copper has been chosen because of its excellent combination of properties, including heat and electrical conduction.

There are several processing techniques by which a copper thin film/alumina substrate system can be formed. Some of the common methods are: sputter coating, vapor deposition, electron beam epitaxy, liquid metal infiltration, solid state diffusion bonding, brazing, and metallization.

Sputter coating is done in a vacuum chamber. The chamber contains a solid copper target that is “sputtered” off the surface by a plasma beam. The sputtered metal atoms are deposited on to the alumina substrate. The sputtered metal atoms deposit on the surface of the alumina substrate and grow together form a continuous layer.

Vapor deposition is also conducted in a vacuum chamber that is resistively heated. The copper is seated in a refractory metal boat or basket until the copper vaporizes in the low pressure atmosphere. The copper atoms then deposit onto the substrate and grow to form a continuous layer.

Electron beam epitaxy also uses a vacuum chamber that contains an electron source and pocket that holds the copper metal to be laid down. An electron beam is focussed on the surface of the copper target. The copper target is bombarded by the electrons, which free copper atoms from the surface creating a stream of copper atoms. The atoms are aimed at the alumina substrate. The atoms deposit on to the substrate forming a layer of copper.

Liquid metal infiltration is a method in which a molten copper metal is imparted to alumina. The alumina is usually in the form of a porous sponge. Alumina that is not fully densified usually serves this purpose. The liquid copper can be injected into the alumina or the ceramic may be dipped in molten metal.

Diffusion bonding is solid state joining process which take place at high temperatures. Bonding temperatures are typically at  $0.8 T_m$  (where  $T_m$  is the melting point of copper) or higher. An inert atmosphere or vacuum is used. To promote contact between the ceramic and the metal, physical stress may be applied by a ram and die. In lieu of a ram, a high pressure atmosphere may be used to create an isostatic pressure state. This process is known as hot isostatic pressing (HIP).

The brazing of ceramic to a metal is similar to soldering of the electrical components. This method uses heat, via a torch, laser, or other heat source, to melt the copper directly to the alumina. A flux may be added to the surface of either material to enhance the liquid metal to ceramic wetting properties.

Metallization pastes use a mixture of fine metal compounds and various volatile compounds that are spread on to the ceramic substrate and fired. On heating the paste, the volatile binders are driven off and the copper remains on the alumina substrate. Copper may also be reaction bonded via a paste to form compounds at the copper alumina interface.

Although there is a wide variety of processing methods available to coat alumina with copper, we can see that all the final products have a common denominator: an interface where the copper and the alumina join. While each method produces an

interface, the physical and chemical structure of each interface is likely to differ considerably. Consequently, the interfaces produced by each method may not behave the same. It is therefore important to know what the characteristics of the interface are.

Thermodynamic and kinetic principles control all the aspects of interface formation, such as, structure, composition, phase formation, and impurity segregation, to name just a few. Let us examine each aspect and its relationship to the interface.

The microscopic structure shows the relationship between the crystallographic and atomistic arrangements at the interface. While the bulk materials have their own structure, the structure of the interface is usually much different from that of the individual bulk materials. The interface structure depends on the thermodynamically and kinetically favorable arrangements that were formed upon fabrication. The structure defines many attributes at the interface, such as coherency and residual stresses. The resulting structure contributes to the interface mechanical, electrical and magnetic behavior.

The interface chemical composition is the result of the chemical stability or instability of the interface. The composition is the result of atomic interactions that are governed by thermodynamic and kinetic responses. In some circumstances, the composition range can vary widely while the interface still retains its desired characteristics. On the other hand, there may be a narrow composition range in which the desired interface properties exist.

Together with the composition and structure, phase formation defines the arrangements of atoms. The phase or phases at the interface are important to the

formation and performance of the interface. As mentioned previously, retention of a phase over a large composition range may allow flexibility in the manufacturing process. On the other hand, the existence of a phase that may occur in a narrow composition range may place many constraints on the manufacturing process.

Impurities are always present in commercial materials, even in high purity (>99.999 %) materials. Impurities tend to segregate to interfaces in order to lower the free energy of the system. While the elimination of an impurity may be impractical, a compromise is to set reasonable limits on the amounts and type of impurities, and to design the process accordingly. The resulting interface may have a few impurities, but performance may not be compromised if the impurities do not cause any appreciable problems. On the other hand, the use of the impurity to favorably modify the interface would be a great asset to engineers.

Studying each aspect requires extensive chemical and crystallographic information. The use of analytical transmission electron microscopy (TEM) has made this process more precise, but the wealth of data collected must also be collated and interpreted. Since there are many aspects to the microstructure, we must examine the data carefully in order to assess the interdependence, if any, between each aspect in relation to the interface microstructure. Finally, there must be correlation between interface microstructure and interface properties. Thus, an understanding of the microstructural aspects of copper-alumina interfaces is required if an optimum combination of these two materials is to be realized.



This study concentrates on characterizing a diffusion bonded copper-alumina interface with emphasis on the distribution of silicon, a common commercial impurity in alumina. The main aims were:

- i) How is silicon distributed in the alumina substrate and what type of bonding environment does it have?
- ii) Is there any phase formation at the copper-alumina interface?
- iii) Does Si diffuse to the metal-ceramic interface?
- iv) If Si is present at the interface, what type of bonding environment does it have?

## II PREVIOUS WORK

Metal-ceramic systems have many commercial applications as discussed in the introduction. As a result there have been many studies on metal-ceramic interfaces. In the case of the copper-alumina system, studies have focused on substrate characterization, interface characterization, and mechanical behavior. A brief review of research on impurities in alumina, characterization of copper-alumina interfaces and mechanical properties of copper-alumina are now presented.

### A. ALUMINA SUBSTRATE

A common impurity in polycrystalline commercial alumina is Si. Often silica is added to the alumina powders as a sintering aid. In addition to Si, other elements have been used as dopants in alumina. There have been several studies on distribution and characterization of impurities in alumina. Kingery (1976) and Brydson (1995) have reported that impurities in alumina tend to segregate to grain boundaries. There have also been studies on the formation of amorphous films at the alumina grain boundaries. Susnitzky and Carter (1990) have examined the structure of grain boundaries in alumina bi-crystals prepared with and without a thin intergranular layer of silica. Their study showed that amorphous silica migrated into pores of alumina during sintering. Kaneko et al. (1998b) have studied segregation effects of Zr impurities in alumina by TEM and EELS. Swiatnicki (1995) has studied intergranular segregation and structure of commercial alumina doped with Ti and Mg in detail with TEM and EDXS. Simpson et al. (1986) have pointed out that the artifacts produced by sample ion milling can give

misleading information about the nature of the interface. They suggest that high resolution electron microscopy must be employed in conjunction with other techniques to obtain unambiguous identification of amorphous grain boundary phases. In the present work the segregation of impurities to various heterogeneous sites were investigated by TEM, EDXS and PEELS.

Kaneko et al. (1998a) have studied the coordination of Si at alumina grain boundaries by means of high resolution electron microscopy and electron energy-loss spectroscopy (EELS). According to Kaneko et al. (1998a), Si is detected within  $\pm 5$  nm of the alumina grain boundaries but not in the grain interior. They also found that Si at the alumina grain boundaries exhibit a six-fold coordination as opposed to four-fold coordination usually exhibited by amorphous forms of silicon oxides and silicates. Hansen et al. (1992, 1994) have examined the coordination of Al and Si in several aluminosilicates by experimental EELS and multiple scattering calculations. The coordination of Si in the alumina grain boundaries and triple junctions as well as at the copper-alumina interface will be examined in the present work and compared with results of these studies.

## **B. COPPER-ALUMINA INTERFACES**

There have been several studies on copper-alumina interfaces in which various processing methods and substrates have been used: diffusion bonding copper to sapphire (Gibbesch and Elssner 1992, Beraud et al. 1989 and Dalglish et al. 1993), electron beam epitaxy of copper on sapphire (Brydson 1995, Rühle 1996 and Scheu et al. 1996), liquid

metal infiltration of copper to alumina (Müllejans and Bruley 1995) and copper-oxygen eutectic (Yoshino 1991, 1992).

TEM and scanning electron microscope (SEM) results from Beraud et al. (1989) showed that in oxygen rich environments CuO could form at the metal-ceramic interface. Trumble (1992) performed a thermodynamic analysis on aluminate formation at copper-alumina interfaces. Rogers et al. (1994) also reported similar results on the role of oxygen at the copper-alumina (single crystal) interface. However the observations of Beraud et al. should not be confused with Brydson (1995) who surmised that oxygen terminated alumina can have interactions with the copper metal that can give rise to PEEL spectra that may be similar to CuO type signatures. Müllejans and Bruley (1993) and Rühle (1996) and Scheu et al. (1996) also reported similar PEELS observations for low  $pO_2$  processing environments. In strong reducing atmospheres CuO was not seen (Dalglish et al. 1993).

The copper-oxygen eutectic method of Yoshino (1991) also reported TEM and SEM results that show copper aluminate readily forms if a CuO paste is calcined on the alumina substrate. Although 96% purity commercial alumina was used, impurities at the interface were not addressed. In a later TEM study by Yoshino (1992), he showed evidence of an amorphous reaction layer formed at the Cu-O eutectic bonded surface.

While all these studies have characterized the interface, they have prepared the interfaces using single crystal alumina or, with the exception of Yoshino (1992) and Beraud (1989), essentially pure alumina.

### C. COPPER-ALUMINA MECHANICAL BEHAVIOR

In addition to interface characterization studies, several mechanical behavior studies have also been reported. Gibbesch and Elssner (1992) asserted that interface strength of an ultra high vacuum bonded copper to polycrystalline alumina could be enhanced by sputter cleaning of the substrates. Holowczak et al. (1991) presented results which showed that calcium, an alumina sintering aid, in conjunction with silicon oxides, lowered copper-alumina peel strength. These bonds were formed with an oxidized copper foil.

Dalgleish et al. (1994) and Tomsia (1993) have carried out mechanical behavior studies on various metals, including copper to alumina substrates, both single crystal and polycrystalline. Tomsia (1993) and Dalgleish et al. (1994) have both postulated that silica enhances metal to alumina bonding process by providing diffusion paths for mass transport and by filling pores at the interface. In Tomsia's work, TEM experiments showed that a thin, continuous amorphous layer of silica was formed at the Pt/Al<sub>2</sub>O<sub>3</sub> interface. Also observed was an increase in bond strength with decreasing levels of alumina purity. Tomsia (1995) has attempted to correlate contact angle and work of adhesion to interface strength.

Dalgleish et al. (1994) showed that mechanical testing of a copper foil diffusion bonded to a polycrystalline alumina substrate showed that failure occurred predominantly in the ceramic. In the same study, copper diffusion bonded to single crystal alumina failed primarily at the interface. Thus, the metal-ceramic interface must have low flaw populations and/or strong chemical bonding (Dalgleish et al. 1994). Crispin and Nicholas

(1989) also reported that failure occurs in the alumina for diffusion bonded copper-alumina (polycrystalline) samples bonded at temperatures greater than 700 °C.

Despite all these elaborate studies, few researchers have critically examined the role of impurities, most notably Si, in alumina on the structure of copper-alumina interfaces and this is the objective of the present work.



### III INSTRUMENTATION

The primary instrument used to study the metal ceramic interface was the conventional transmission electron microscope (CTEM), in conjunction with two characterization techniques: parallel electron energy loss spectroscopy (PEELS) and energy dispersive x-ray spectroscopy (EDXS).

When high energy (200 KeV) electrons traverse through a thin foil material, a number of excitations result from the transfer or loss of energy of the incident electrons. Figure 3.1 illustrates the most important electron – specimen interactions that occur as an electron beam passes through a TEM sample. The excited states in the material decay by emission of x-rays, secondary and Auger electrons, photons etc. Since basic principle information on CTEM, PEELS, and EDXS is readily available, this section will concentrate on how EDX and PEEL spectra are interpreted with particular emphasis on detectability limits and sources of error.

#### A. EDXS

##### 1. General EDXS

EDXS systems have been available as optional equipment on CTEM, since the mid 1970's. The ability to detect elements quickly while imaging has made EDXS an extremely useful tool for qualitative as well as quantitative analysis. Among the interactions that occur while an electron beam passes through a sample, the characteristic x-rays generated can be easily monitored.



Characteristic X-rays are given off when an electron transitions to a lower energy state (de-excitation event), e.g. an inner electron is inelastically scattered by the passing electron beam and is replaced by an outer shell electron. Since, the energy is directly

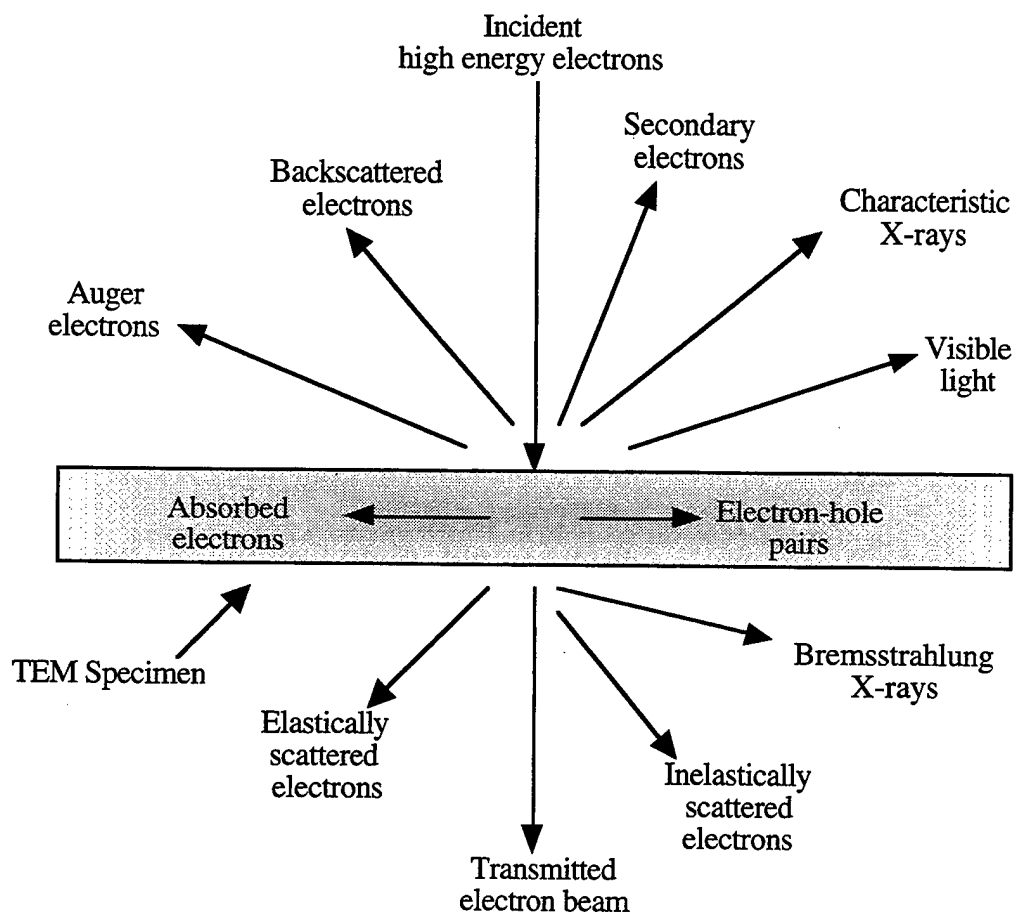


Figure 3.1 Signals resulting from the interaction of a high energy electron beam with a thin foil material (after Williams, D. B. and Carter 1996).

proportional to the type of transition in each element, we can associate several energy peaks to a particular element. Hence, we can assign K, L, & M, to each peak for each transition to a particular orbital and the subscripts  $\alpha$  and  $\beta$  to each letter to indicate transitions within the given orbital. Figure 3.2 is an EDX spectrum for copper. The spectrum shows counts versus energy. The counts represent the number of x-rays counted at a given energy. The K and L peaks are labeled in Figure 3.2.

In the CTEM, the electron beam passes through the sample and the generated x-rays are collected by a p-i-n semiconductor detector, usually Si-Li, which is usually located above the sample. The x-rays that hit the semiconductor will generate electrons or holes, the number of which is directly proportional to the energy of the incoming x-ray. The electrons and holes are separated by the internal reverse bias of a very narrow p-n junction. This results in a charge pulse proportional to the x-ray energy. The voltage is then amplified, using a field effect transistor. The signal is then stored in a multi-channel array and displayed on a computer screen as counts versus energy. The detection is performed serially; thus, resulting in spectra that is dispersed in energy. The collection process can be done while imaging or with a probe. The small probe spot sizes associated with a CTEM with STEM capability can provide high spatial resolution EDXS analysis and imaging. (Williams and Carter 1996)

## **2. Sources of error in EDXS**

The acquisition of quality EDX data is quick and easy, provided proper precautions are taken. There are four key points that deserve attention:

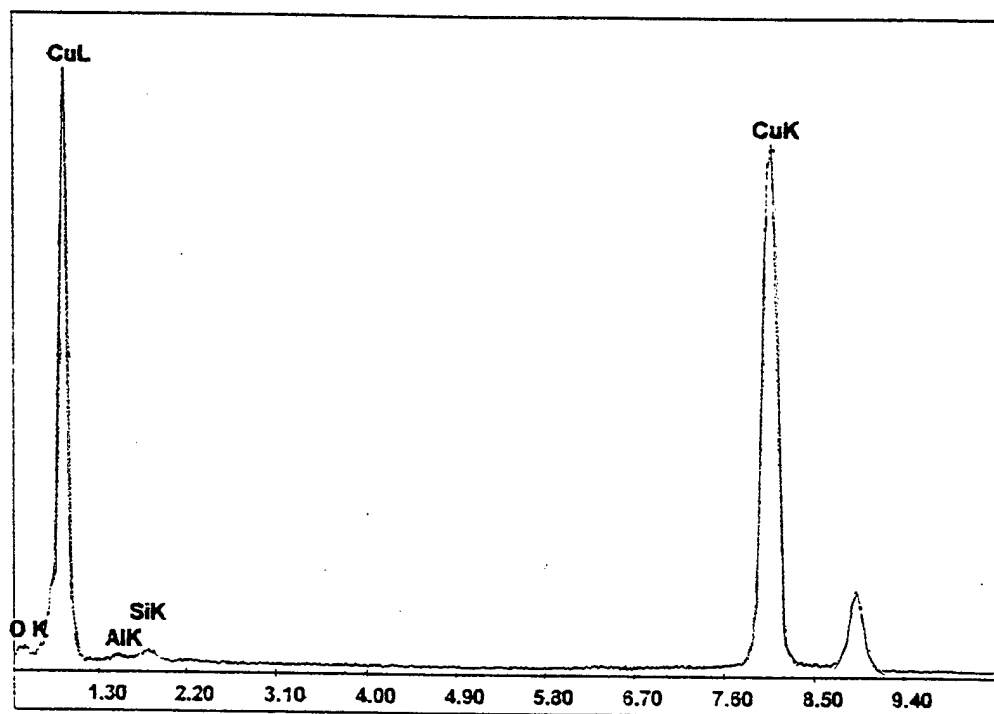


Figure 3.2 is an EDX spectrum for copper. Note: L and K lines are indicated (all EDX spectra in this thesis are shown counts, vertical scale, versus energy (KeV)).

- i) X-ray contributions by the holder, sample grid, and column.
- ii) Beam spreading in the specimen.
- iii) Detector limitations: dead time (saturating the detector).
- iv) Artifacts in the spectra: contributions due to the detector by itself and escape peaks.

The first point that deserves attention is the location of the sample within the CTEM. The x-rays that are collected, generated from a given area may have contributions from the sample holder, sample support grid (if used), column, etc. In order to minimize stray x-ray contributions, one must adhere to manufacturer's recommendations regarding sample position: x, y and z coordinates and tilt(s) with respect to the detector. Sample grid type should be chosen carefully in order to avoid or minimize detection of unwanted elements that appear in the grid material.

The second point is subtle, but very important. Although the beam and the probe sizes in a CTEM are quite small compared to that of a SEM, one must keep in mind that the beam has a point spread function. The location of the beam with respect to the sample features must be carefully chosen to avoid unwanted contributions from surrounding areas. Spatial as well as quantitative results can easily be compromised if the feature in question is of the order of the same size as the beam. A quantified analysis for beam size is covered in detail in the section on spatial resolution in EDXS.

The third point addresses the way in which one collects data. While high count rates are desirable to produce better counting statistics, the semiconductor detector has limitations on its throughput. This is quantified by the dead time value. The dead time is

defined as the time between samplings of the input stream. A practical dead time upper limit for a Si-Li detector is less than 30%. The number of counts will depend on sample thickness and atomic number, electron beam current and probe size. There is compromise between higher counts and beam damage to the sample. The higher the currents and longer the counting times, the greater the likelihood of sample damage. Caution must be exercised to prevent beam damage to the sample while trying to maximize counts while maintaining an acceptable dead time.

The fourth point is concerned with the interpretation of the peaks in the acquired spectra. There are two common peaks other than the regular characteristic peaks: self-generated characteristic peaks caused by the detector and escape peaks. A self-generated characteristic peak is caused by the excitation of x-rays within the detector by the incoming signal from the sample. In the case of a Si-Li detector, a small Si peak may appear in the acquired spectra. The peak intensity is usually small, less than 0.5%. The silicon peak can easily be dismissed in samples where there is no known silicon present. The difficulty arises in samples in which silicon is present in small amounts. As a result, careful analysis of the spectral data is needed to assure the validity of low intensity peaks of elements that are part of the detector composition. The second common peak type is the escape peak. Escape peaks are generated when two characteristic x-rays of the same energy hit the detector simultaneously. The result is a peak that is twice the energy of the original x-rays. The concern arises when the escape peak is close in energy to the characteristic x-ray energy of another element that is to be detected.

### 3. Spatial resolution in EDXS

As mentioned previously, although beam spreading is considerably smaller in the TEM than in the SEM, it still occurs. There are several models for determining spatial resolution which takes into account beam spreading, the simplest being the Reed model which gives the following equation for the spread,  $b$  (cm):

$$b = 625 (\rho/A)^{1/2} (Z/E_0) t^{3/2} \quad (3.1)$$

where

$E_0$  = accelerating voltage (kV)

$Z$  = atomic number

$A$  = atomic weight

$t$  = thickness (cm)

$\rho$  = density ( $\text{g cm}^{-3}$ ).

$b$  is related to  $d_i$ , the initial beam diameter, by:

$$d_{\text{spread}} = d_i + b \quad (3.2)$$

This diameter can be further refined by taking the average diameter since there is no spread at the surface and the maximum spread,  $d_{\text{spread}}$ , occurs upon exiting the sample.

The final beam diameter being:

$$d_{\text{average}} = (d_{\text{spread}} + d_i)/2 \quad (3.3)$$

### 4. EDXS quantification methods

Having developed an approximation for the sample volume in which x-rays are excited, the EDXS spectra can be quantitatively analyzed. The algorithms applied to the

raw spectra are known as ZAF corrections, where Z represents atomic number, A the absorption, and F the fluorescence. Essentially, the algorithms consider sample thickness, sample density, k-factors (Cliff-Lorimer factors), the sample average atomic number (Z), the absorption and fluorescence of x-rays by nearby atoms in calculating the atomic percentages of the elements present. Computer programs are supplied by detector manufacturers to carry out these calculations.

## **B. PEELS**

### **1. General PEELS**

The advent of superior electronics has made the PEELS for TEM a commercially viable device since the late 1980's and it has gained popularity in the 1990's as an effective means to obtain spatial distribution of elements as well as chemical bonding information.

In PEELS, the primary information comes from the excitations unlike most spectroscopies (like EDXS) which extract information from the deexcitation process. The PEEL spectra are thus derived from the electrons that have passed through a thin foil sample and lost energy.

Figure 3.3 shows the three energy regions of the electron energy loss spectrum that are of interest: a zero loss peak, low loss region, and high loss region. The zero loss peak contains mostly forward scattered electrons that have not undergone discernable energy loss. It thus includes phonon losses which are of the order of 1/40 eV. The low loss region contains electrons that have interacted with the outer most electrons of the

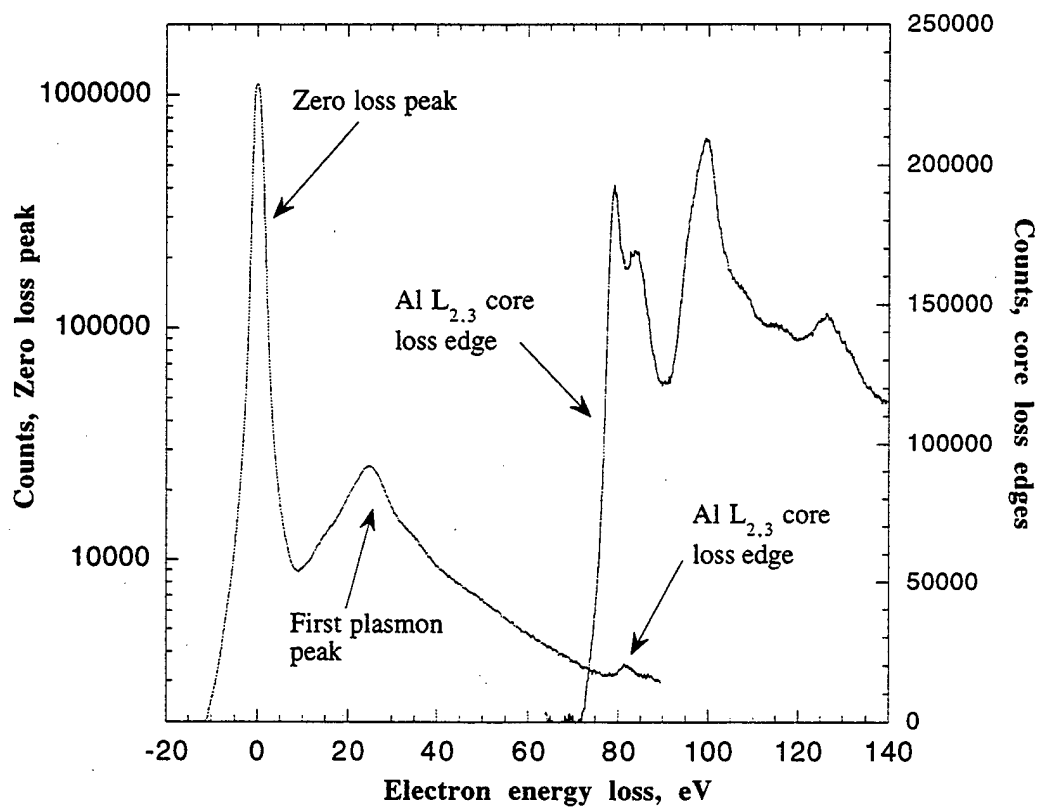


Figure 3.3 A typical electron energy loss spectrum with the three energy loss regions indicated: a zero loss peak, low loss region, and high loss region.



the atom. These electrons generate plasmon oscillations in the weakly bound electrons of the atom. The high loss regions contain the electrons that have interacted with the inner-shell atom electrons causing ionization. The energy associated with the inner shell excitation is equal to the difference between the Fermi energy and the binding energy associated with the particular inner shell. These excitations result in an inner shell loss edge and provide a very convenient method for the performance of quantitative chemical analysis and to identify and study the bonding features associated with the particular atom in the material.

There are dedicated PEELS devices but a recent development has enabled PEEL images to be generated as well as spectra. The Gatan PEELS Imaging Filter (GIF) is unique in that it can function as a conventional PEELS and as an imaging device. The electrons pass through the sample and go through an aperture. After the aperture, the electrons are directed through a magnetic prism, in which the energy loss can be separated. The dispersed stream of electrons is then passed through a quadrupole in order to focus spectrum or project an image on to a CCD detector. The result is the collection of energy-dispersed spectrum or an energy filtered image.

Since a range of energy losses is collected simultaneously, the procedure is called parallel electron energy loss spectroscopy. The use of a parallel detection makes collection times relatively short compared to those associated with EDXS, thus making acquisition easier for the operator as well as possibly reducing sample damage.

PEELS can be carried out in probe mode or image mode. In the probe mode (which is most often used) spectra can be acquired from specific areas of a sample and

the data can be evaluated. The spectrum from a PEELS probe is a signature of the atomic environment of the atoms being illuminated by the electron beam. The ionization edges in the spectrum are also proportional to the number of atoms that have interacted with the electron beam.

## **2. Sources of error in PEELS**

There are several sources of error when collecting PEEL spectra and images. When collecting spectra the samples have to be reasonably thin. An accepted range is when the ratio of the sample thickness,  $t$ , to average mean free path which the incident electron travels,  $\lambda$ , (i.e.,  $t/\lambda$ ) is  $< 1.5$ . Samples that are too thick will cause the electrons to scatter multiple times creating artifacts in the PEEL spectra. If thick samples are unavoidable, multiple scattering corrections should be applied. The quality of the sample is important especially in interface studies. The alignment of the interface with the electron beam is critical when taking PEEL images. Care should be exercised when trying to establish the width of features and elemental concentrations, as a tilted boundary may exaggerate the width and the sample thickness variations may lead to concentration variations. Although acquisition times for PEELS are relatively short compared to that of EDXS, samples may still be damaged by the electron beam. Sample beam damage may also cause artifacts in the PEEL spectra (Kaneko, personal communication, 1997). In addition, long acquisition times may flood the CCD causing blooming, which may also lead to artifacts in both spectra and images.

### C. COMPARISON OF DETECTABILITY AND SPATIAL RESOLUTION FOR EDXS AND PEELS

There are several factors that are important to consider when comparing EDXS and PEELS. The main concerns are specimen survival verses information required. Beam damage is always a concern when acquisition times are long. Since PEEL spectra and maps are collected in parallel, the acquisition times are in general much shorter than for EDXS. However, heavy elements ( $Z > 26$ ) can be quickly acquired in EDXS and hence beam damage is less of a problem.

Leapman and Hunt (1991) presented results that indicate that PEELS is the desired method for detecting elements with atomic number,  $Z < 10$  and EDXS is the method of choice for  $10 < Z < 25$ , when using K edges (lines). However, PEELS has higher sensitivity for  $10 < Z < 25$  if  $L_{2,3}$  edges are used. For  $Z > 26$  the best sensitivities of both PEELS and EDXS become comparable.

The information required may dictate the need for each technique. In some cases, there may be considerable overlap in the peaks or edges for EDXS and PEELS, respectively. For copper-alumina interfaces, the Cu- $M_{2,3}$ , Al- $L_{2,3}$  and the Si- $L_{2,3}$  edges are in the same energy range of 50 eV to 150 eV. In EDXS  $K_{\alpha}$  peaks for Si (1.740 KeV), Cu (8.047 KeV) and Al (1.487 KeV) peaks do not overlap and this, of course, is an advantage.

The spatial resolution of EDXS is limited by beam spreading in the sample, whereas in PEELS the illuminated area from which the energy loss information comes is

essentially the same size as the incident probe size. So for the same size incident probe PEELS has a superior spatial resolution.

#### D. SPATIAL DIFFERENCE TECHNIQUE

While obtaining PEEL spectra from a homogeneous region is relatively straightforward, obtaining PEEL spectra from an interface is considerably more challenging. In the case of the copper-alumina interface, the PEELS probe will encompass a section of the interface and the two surrounding bulk areas. As a result, the electron energy loss near edge fine structure (ELNES) of the interface is present along with the contributions of bulk copper and bulk alumina. If the edges in question do not overlap, then information can be directly viewed in that section of the spectra. However, if the edges overlap, the interface contribution must be deconvoluted. As mentioned in the previous section, the edges for the Cu-M<sub>2,3</sub>, Al-L<sub>2,3</sub> and the Si-L<sub>2,3</sub> overlap in the 50 to 150 eV region. Müllejans and Bruley (1993, 1995) have developed the Spatial Difference technique in order to remove contributions from surrounding bulk materials in interface spectra. The method can be written in the formula:

$$SD = I_{\text{Interface}} - ( f_{\text{Copper}} I_{\text{Bulk Copper Reference}} + f_{\text{Alumina}} I_{\text{Bulk Alumina Reference}} ) \quad (3.4)$$

where

SD = Spatial Difference

I<sub>x</sub> = The intensity of spectrum from component x (the components for copper, alumina and interface are shown in the equation above)

$f_x$  = The fractional amount, i.e. contribution of component x.

Determination of the fractional contributions of the bulk reference spectra should follow these guidelines. First, strong reference edge features that are present in the raw interface spectra should be minimized in the SD. Secondly, if there are chemical shifts present in the raw interface spectra, the edge on set, as defined by the reference spectra, should be minimized. Finally, There should not be any negative counts in the SD where there is signal. (Rühle 1996)

#### IV EXPERIMENTAL

A Cu-Al<sub>2</sub>O<sub>3</sub> interface was created under vacuum by diffusion bonding of 100  $\mu$ m copper foils (99.999% purity) pressed between polished polycrystalline alumina substrates (~99.5% purity) for several hours at ~90% of the melting temperature of copper. In addition to the vacuum environment, graphite furniture was used to minimize oxygen partial pressure, thus reducing the possible formation of oxidation products at the metal ceramic interface.

TEM samples were made from the bulk interface samples. The large blocks were sectioned with a diamond blade in a slow speed saw into beams (approx. 25.4 mm x 4.0 mm x 4.0 mm, with interface centered, perpendicular to the length of the beam). Smaller samples (approximately 1.0 mm x 3.0 mm x 3.0 mm) were sectioned from the beams. The resulting samples were mounted to a grinding/polishing "stub" using a low melting (acetone soluble) mounting wax. The sample was thinned on one side using SiC grinding paper (ANSI 500, 800, 1000, 2500, 4000 grits), polished by diamond paste (water soluble, 1  $\mu$ m and 6  $\mu$ m on Buehler microcloth) and finally finished with colloidal silica (0.05  $\mu$ m, on Buehler microcloth). The sample was then floated off in solvent and remounted on the other side. After completion of polishing, a 3 mm outer diameter copper grid (inner diameter was either a 2 mm hole or a 1 mm x 2 mm slot) was attached to the sample using silver dag. The polished samples had a thickness <25  $\mu$ m. The samples were further thinned using a Gatan Ion Miller (low angle holder: 9 degrees, 6

keV, 1 amp) or Gatan PIPS (6 degrees and 6 keV and 1 amp). Samples were milled till perforation.

The samples were examined in a Topcon 002B TEM, operating at 200kV, equipped with an EDAX EDXS system (ultra thin window) and a Gatan PEELS Imaging Filter. The EDXS software used was DX4 and the PEELS software was EL/P 3.0. The EDX spectra, taken with 16 nm probes, were used to establish the distribution of silica in the bulk alumina and at the interface. PEEL spectra, taken with 6 nm probes, were used to characterize coordination effects of elements in the bulk alumina and at the Cu-Al<sub>2</sub>O<sub>3</sub> interface. The interface PEEL spectra were further analyzed using the spatial difference technique (Müllejans and Bruley 1995) in the analysis of interfaces. Because the probe encompassed the interface plus neighboring bulk regions, appropriate proportions of bulk copper and bulk alumina spectra were subtracted from the interface spectra.

## V RESULTS AND DISCUSSION

The copper-alumina samples were examined using conventional TEM imaging, EDXS and PEELS. Initial observations were carried out on a scanning electron microscope. Figure 4.1 shows a low magnification SEM image of the copper-alumina interface. As shown in Figure 4.1, the copper grain size was approximately 20  $\mu\text{m}$ , and was of the order of the film thickness. The alumina grain size was in the range of 1  $\mu\text{m}$  to 5  $\mu\text{m}$ , resulting in many triple junctions and numerous grain boundaries. As seen in Figure 4.1, there was cutting/polishing damage evident in the alumina and at the metal-ceramic interface. There were many grain boundaries in the alumina that intersected with the copper-alumina interface. Also, there were some alumina triple junctions that were close to the Cu-alumina interface.

Following these initial observations, the study was continued using the TEM, with concentration on two areas, the alumina substrate and the copper-alumina interface. Figure 4.2 is a bright-field TEM micrograph of a typical metal-ceramic interface area and an adjoining alumina triple junction. Since silica is known to segregate to the triple junctions and grain boundaries in alumina during sintering (Kingery et al. 1976), the triple junctions and grain boundaries in the alumina were examined to establish the nature and distribution of silicon in the alumina substrate. The copper-alumina interfaces were also examined to search for possible segregation of Si along the metal-ceramic interface.



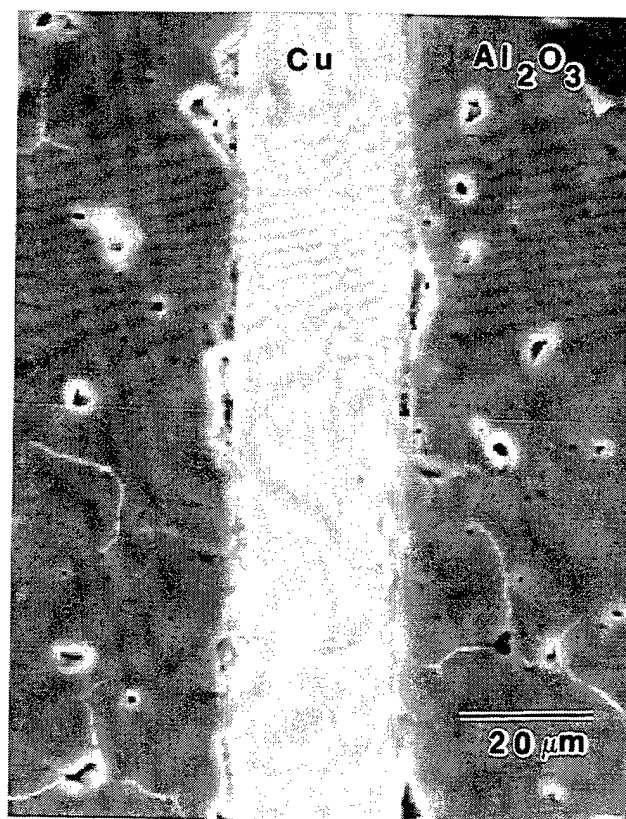


Figure 4.1 Low magnification scanning electron microscope micrograph of the copper-alumina interface. Note: polishing damage at the interface.

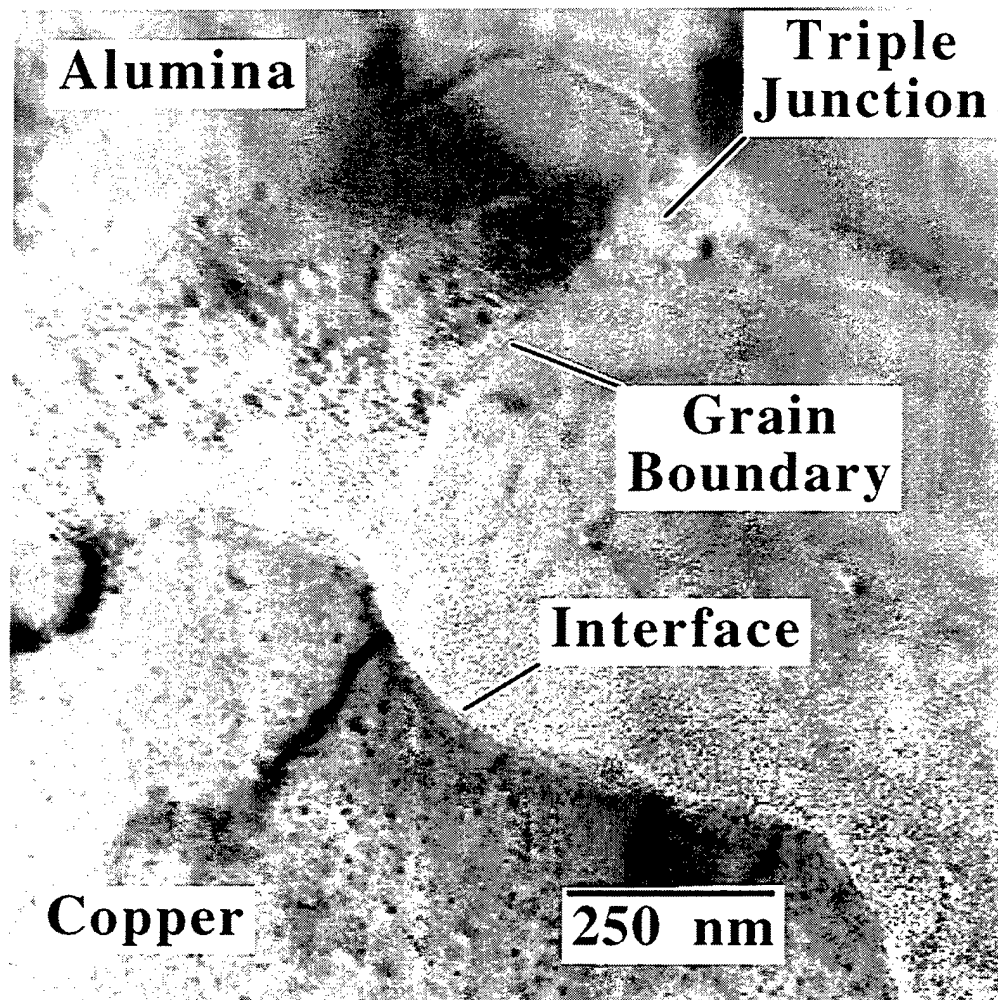


Figure 4.2 Bright-field TEM micrograph of the copper-alumina interface.

## **A. ALUMINA SUBSTRATE**

### **1. Imaging**

Various triple junctions and grain boundaries in alumina were examined in detail. Figure 4.3 is a bright-field TEM micrograph of a typical triple junction in the alumina. As seen in this Figure, triple junctions in alumina were completely occupied by another phase(s). The rest of the grain boundaries in alumina away from the triple junctions did not show the presence of any other phases. Figure 4.4 is a microdiffraction pattern (3 nm probe) taken from the middle of a typical triple junction, point A in Figure 4.3. The microdiffraction pattern shows a mixture of a crystalline phase (spots) and a glassy phase (broad diffuse ring). The pattern also had many spots making an unambiguous indexing impossible. However, it is evident that the crystalline phase is in the form of very fine particles.

### **2. EDXS**

EDXS was used to determine the distribution of Si in the alumina substrate. EDXS was carried out in probe mode. Probe sizes varied from 6 nm to 16 nm as discussed in the experimental section. The EDX spectra were quantified under several conditions to determine the maximum variance caused by changes in ZAF inputs by varying specimen thickness and sample density. Figures 4.5 shows the quantitative results from an  $\text{Al}_2\text{O}_3$  grain boundary area for sample thickness of 50 nm and 25 nm respectively. The results show that a 50% variation in foil thickness caused a maximum 0.5 at. % change in the elemental compositions. Figure 4.6 shows quantitative EDX results from alumina grain

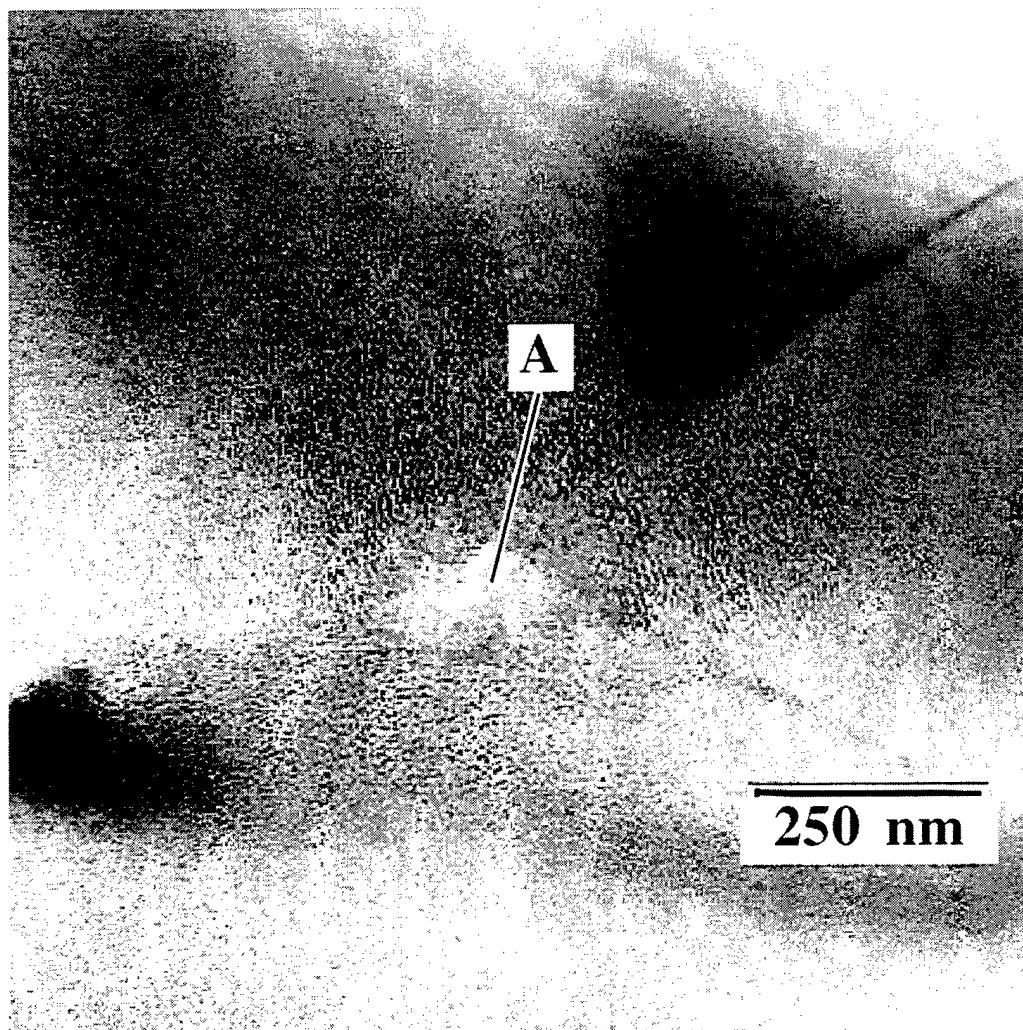


Figure 4.3 Bright-field TEM micrograph of a typical alumina triple junction. Point "A" denotes the probe position for the microdiffraction pattern given in Figure 4.4

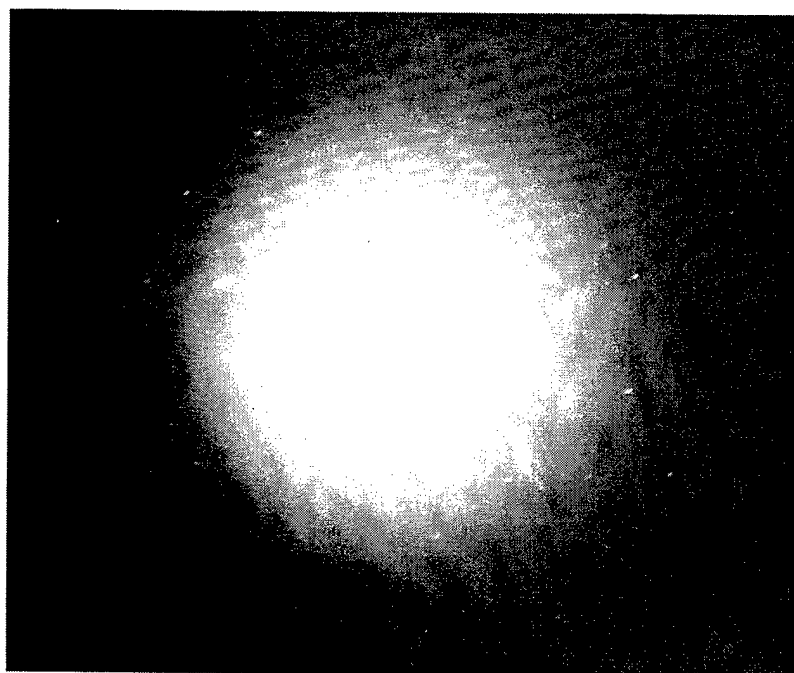


Figure 4.4 Microdiffraction pattern from point “A” in Figure 4.3, note: diffuse ring (amorphous phase) as well as sharp spots (crystalline phase).

**A:\HASH10.SPC Label :**

**kV : 200.00    X Tilt : 10.00    Y Tilt : 0.00    Azimuth : 0.00**

**Elevation : 17.60    Tc : 40**

**Detector Type : SUTW    Resolution : 138.73    Lsec : 170**

**Thin Apx, Abs Corr**

**Theoretical KAB, Elements, Model : Zaluzec□□**

**Foil thickness = 50 nm**

Element	Weight %	Atomic %	Xpt
O K	28.0	48.7	0.931
AlK	32.8	33.8	0.499
SiK	0.6	0.6	0.539
CuK	38.6	16.9	0.008
Total	100.0	100.0	

**Inc Angle = 90.00    Abs Path = 318.85**

**Density = 6.45    Iter = 3**

Element	Net Inte.	Bkqd Inte.	Inte. Error	P/B
O K	15.82	0.71	1.97	22.41
AlK	58.90	0.94	1.01	62.58
SiK	0.89	0.97	11.77	0.92
CuK	41.64	0.19	1.19	221.19

**A:\HASH10.SPC Label :**

**Foil thickness = 25 nm**

**kV : 200.00      X Tilt : 10.00      Y Tilt : 0.00      Azimuth : 0.00**  
**Elevation : 17.60   Tc : 40**  
**Detector Type : SUTW   Resolution : 138.73   Lsec : 170**

**Thin Apx, Abs Corr**  
**Theoretical KAB, Elements, Model : Zaluzec□□**

<b>Element</b>	<b>Weight %</b>	<b>Atomic %</b>	<b>Xpt</b>
O K	26.1	46.6	0.631
AlK	32.4	34.4	0.343
SiK	0.6	0.6	0.365
CuK	40.9	18.4	0.006
Total	100.0	100.0	

**Inc Angle = 90.00    Abs Path = 212.57**  
**Density = 6.45    Iter = 3**

Figure 4.5 ZAF corrected EDXS results from triple junction center for 50 nm and 25 nm thickness.

Thin Apx, Abs Corr				
Theoretical KAB, Elements, Model : Zaluzec□□				
Element	Weight %	Atomic %	Xpt	
O K	38.2	51.8	0.092	
AlK	14.6	11.7	0.016	
SiK	47.2	36.5	0.019	
Total	100.0	100.0		
Inc Angle = 75.00 Abs Path = 44.82				
Density =3.97 Iter =2				
Element	Net inte.	Bkgd Inte.	Inte. Error	P/B
O K	8.16	0.12	2.48	68.79
AlK	8.67	0.15	2.41	58.43
SiK	23.73	0.16	1.45	145.45

Thin Apx, Abs Corr				
Theoretical KAB, Elements, Model : Zaluzec□□				
Element	Weight %	Atomic %	Xpt	
O K	38.2	51.8	0.088	
AlK	14.6	11.7	0.016	
SiK	47.2	36.5	0.018	
Total	100.0	100.0		
Inc Angle = 75.00    Abs Path = 44.82				
Density = 3.79    Iter = 2				
Element	Net Inte.	Bkgd Inte.	Inte. Error	P/B
O K	8.16	0.12	2.48	68.79
AlK	8.67	0.15	2.41	58.43
SiK	23.73	0.16	1.45	145.45

Figure 4.6 ZAF corrected EDXS results from triple junction center (foil thickness 25 nm) for densities of 3.97 g/cm<sup>3</sup> (alumina) and 3.79 g/cm<sup>3</sup> (silica).

boundary area for sample densities  $3.97 \text{ gm cm}^{-3}$  (100%  $\text{Al}_2\text{O}_3$ ) and  $3.79 \text{ gm cm}^{-3}$  (100%  $\text{SiO}_2$ ) respectively for 100 nm thickness. The results show that sample density changes did not cause any change in the elemental compositions. In summary, the analysis showed that the thickness variations and density variations accounted for a 0.5 at. % and 0.01 at. % maximum variance respectively. Oxide calculations were also carried out with similar results in variance. However, the oxide calculation program assumes that all elements are 100% oxidized with no monoatomic species or mixed oxide states.

EDXS from the interior of the alumina grains showed no impurities or Cu. Silicon was found on some grain boundaries and all triple junctions. Figure 4.7 and 4.8 show the EDX spectra taken from the center of a triple junction and from an adjoining grain boundary, respectively. Figure 4.7 and 4.8 clearly show Si counts. Typically the Si concentration was highest at the center of the triple junction and dropped to below detectable limits at  $\sim 0.5 \mu\text{m}$  along an adjoining grain boundary. The quantitative results are given for the spectra from the triple junction in Figure 4.9 for a sample thickness of 25 nm and a density of 3.83 (25 wt. %  $\text{Al}_2\text{O}_3$  and 75 wt. %  $\text{SiO}_2$ ) for the atomic species. The highest Si concentration was measured to be 36 at. % at the center of the triple junction. Figure 4.10 shows a bright field TEM micrograph of an alumina triple junction. EDX spectra were collected from the center of the triple junction and along the indicated grain boundary, using 6nm probe. Quantitative analysis of the spectra for Al and Si were performed. Figure 4.11 is a plot of the Si:Al ratio (at. %/at. %) as a function of distance from the center of the triple junction along a grain boundary. The ratio varied from 2.5 to 0.6, the higher silicon concentrations being measured near the center of the triple



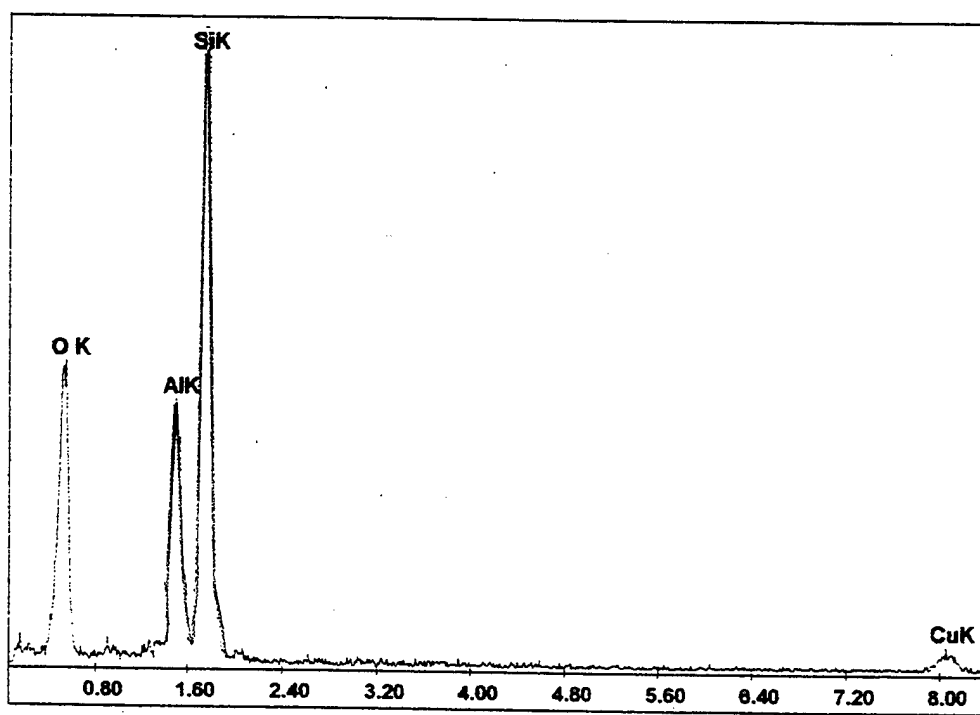


Figure 4.7 EDX spectrum taken from the middle of an alumina triple junction as discussed in the text.

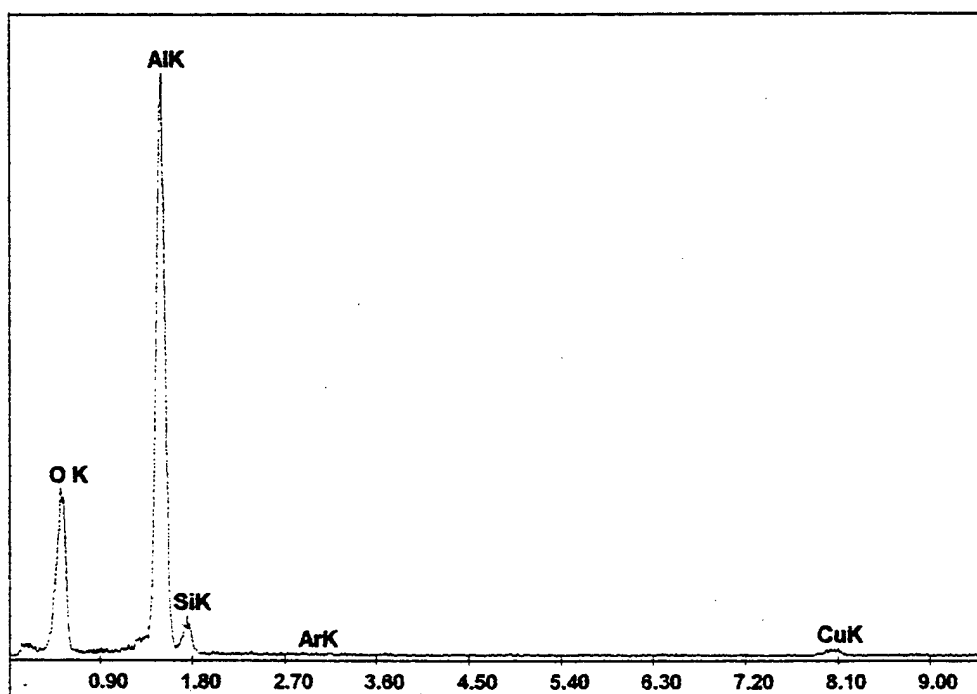


Figure 4.8 EDX spectrum from an alumina grain boundary near a triple junction.

Thin Apx, Abs Corr				
Theoretical KAB, Oxides, Model : Zaluzec				
Element	Weight %	Atomic %	Xpt	
Al2O3	21.5	13.9	0.005	
SiO2	78.5	86.1	0.010	
Total	100.0	100.0		
Inc Angle = 90.00   Abs Path = 53.14				
Density = 3.83   Iter = 1				
Element	Net Inte.	Bkgd Inte.	Inte. Error	P/B
AlK	3.67	0.15	2.41	58.43
SiK	23.73	0.16	1.45	145.45

Figure 4.9 ZAF corrected EDXS oxide results from the middle of the triple junction for thickness of 25nm shown in Figure 4.3.

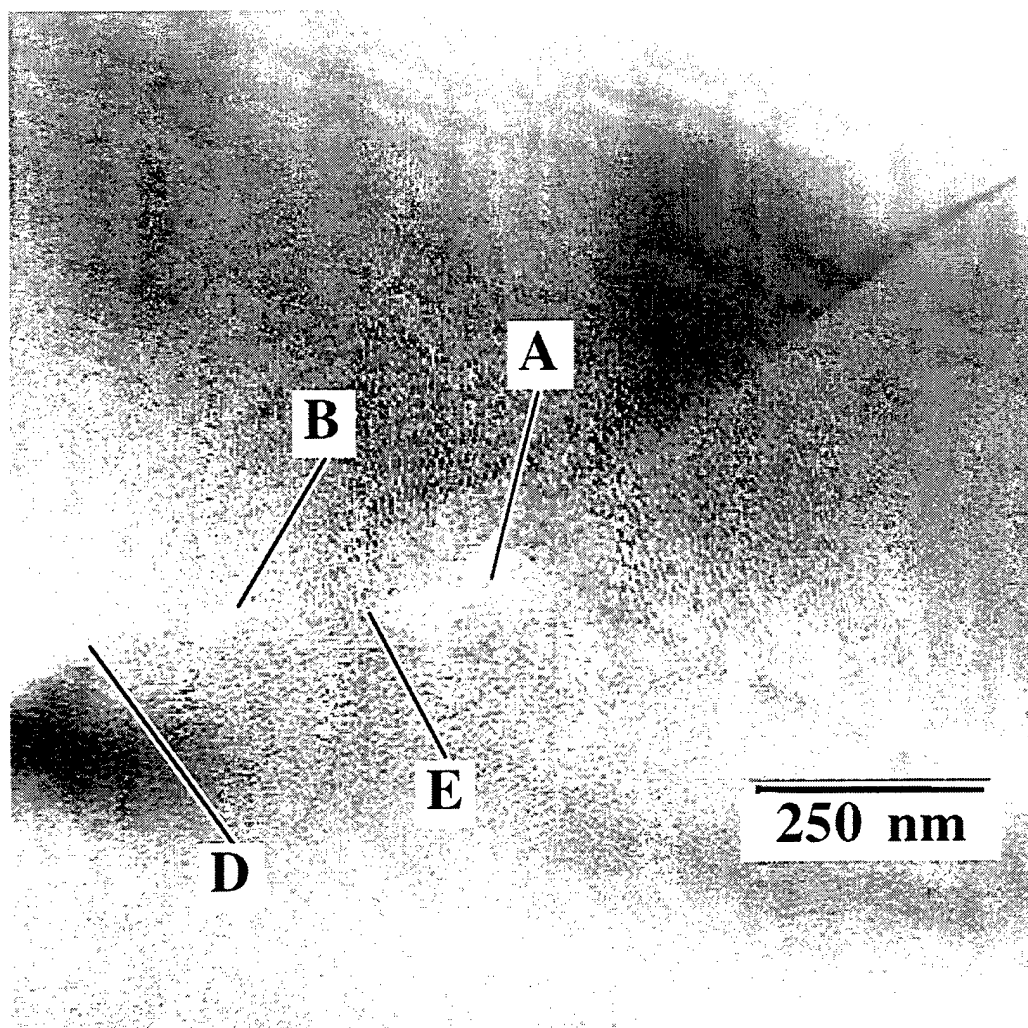


Figure 4.10 Bright-field TEM micrograph of the triple junction. Letters denote EDXS probe positions given in Figure 4.11.

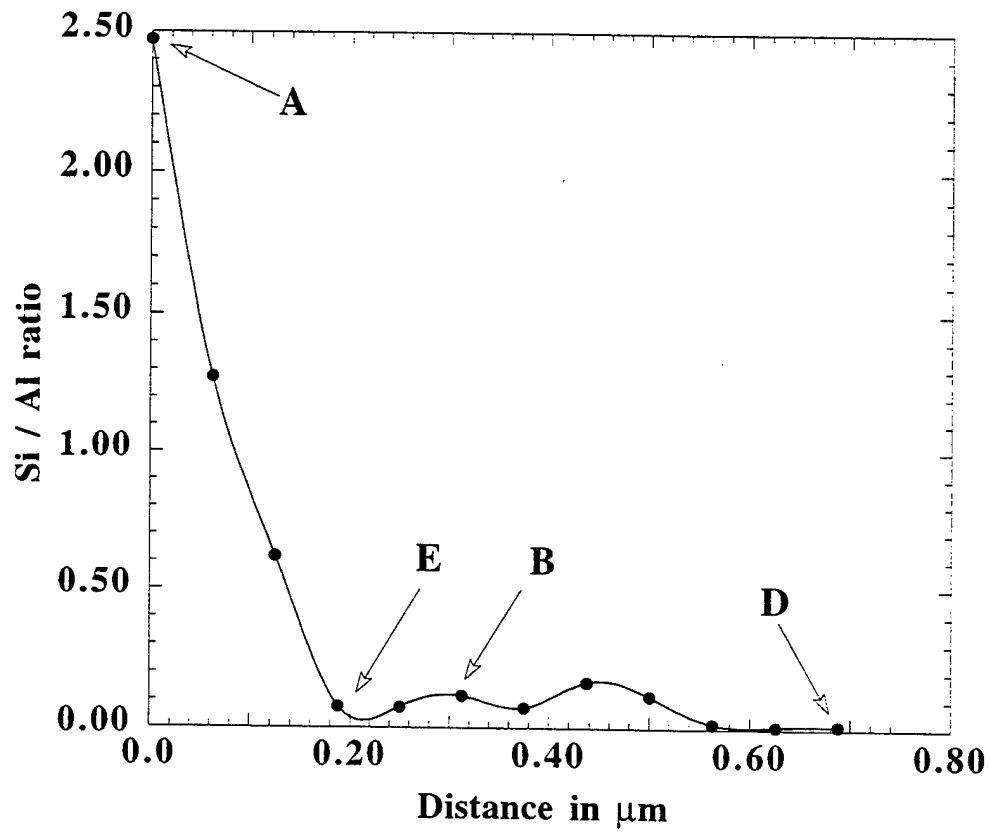


Figure 4.11 Plot of the Al:Si ratio as a function of distance along a grain boundary from the triple junction. Letters correspond to those indicated in Figure 4.10.

junction. Silicon was detected to distances approximately 0.5  $\mu\text{m}$  along the grain boundary. There was no evidence of silicon in the alumina grains that formed the triple junction as seen in Figure 4.12 which is a typical EDX spectrum from an alumina grain and Figure 4.13 shows the corresponding quantitative results for that spectrum.

Quantitative EDXS analysis for oxides from the center of the triple junction showed the composition to be  $26.0 \pm 0.5$  wt. %  $\text{Al}_2\text{O}_3$  and  $74.0 \pm 0.5$  wt. %  $\text{SiO}_2$ . According to the phase diagram, Figure 4.14, mullite (approximately 60 wt. % alumina and 40 wt. % silica) and a silica solid solution phase can coexist when the alumina content is below  $\sim 72.0$  wt. %. Thus, the experimentally determined composition at the triple junction using EDXS suggests a mixture of two phases, mullite and silica. This result is in agreement with the observed micro diffraction pattern (Figure 4.4). The d-spacings of the spots in the diffraction patterns are consistent with mullite and the radius diffuse ring with the expected position of the glassy "hump" associated with glassy silica.

### 3. PEELS

PEELS was carried out to obtain bonding information from the various regions in the alumina substrate. PEELS was performed in diffraction coupled mode. Zero loss spectra were taken before and after recording all core loss PEEL spectra. The core loss spectra were then calibrated for energy scale using the zero loss peaks. Figure 4.15 shows a typical zero loss peak before acquisition and an overlaid zero loss spectra after acquiring core loss spectra. This was done to confirm that there was not substantial energy shifts which might cause errors in edge position. As Figure 4.15 shows, there is

some shift in energy scale, but the shifts proved to be minimal, the largest energy shift being  $< 0.2$  eV.

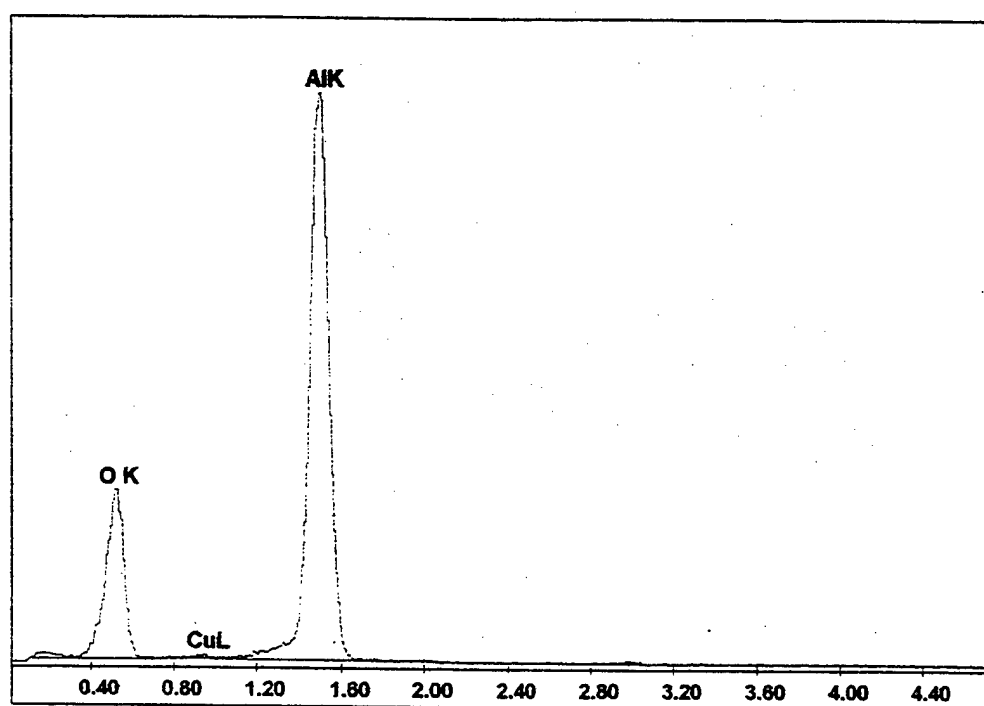


Figure 4.12 EDX spectrum from an alumina grain interior.

Thin Apx, Abs Corr			
Theoretical KAB, Elements, Model : Zaluzec□□			
Element	Weight %	Atomic %	Xpt
O K	50.9	63.6	0.114
AlK	49.1	36.4	0.032
Total	100.0	100.0	
Inc Angle = 90.00 Abs Path = 82.68			
Density = 3.79 Iter = 2			

Figure 4.13 ZAF corrected quantification of EDXS spectrum shown in Figure 4.12.



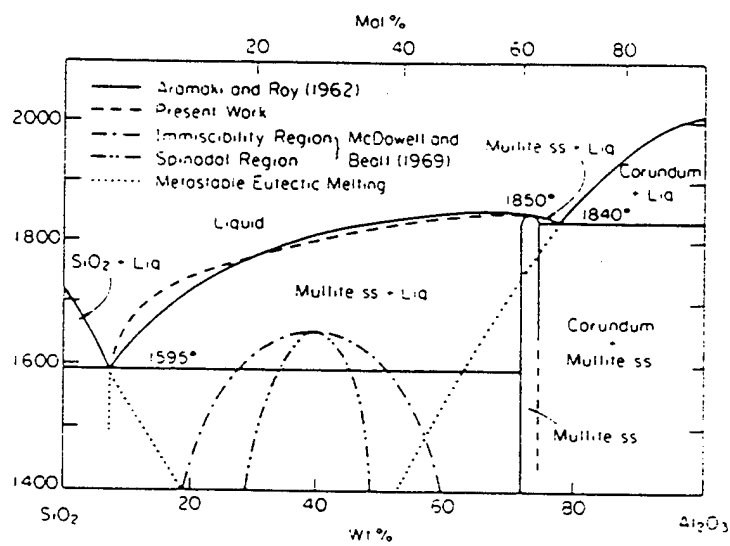


Figure 4.14 Alumina-Silica phase diagram (Davis and Pask 1972).

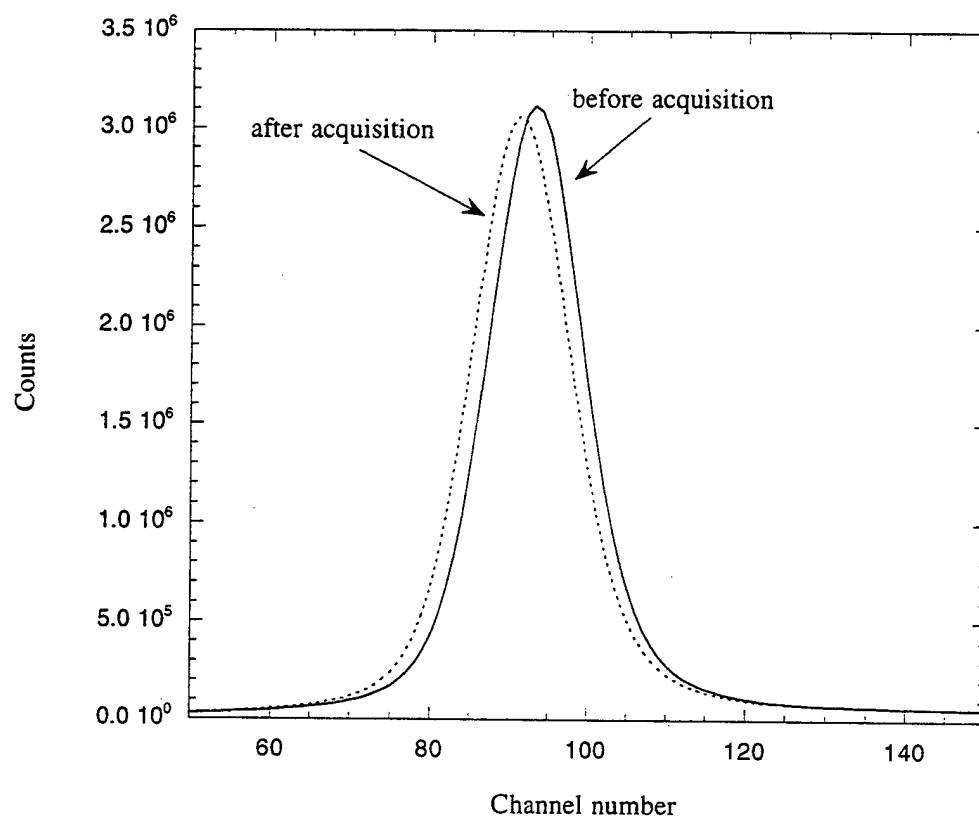


Figure 4.15 PEEL spectra overlay of zero loss peak before and after core loss spectrum collection. Note: only 1-2 pixel shift.

PEEL spectra from the center of the triple junction and adjacent alumina grains were acquired at 0.1eV energy resolution in the 50eV to 150eV range, including the Al- $L_{2,3}$  edge and Si- $L_{2,3}$  edge. Figure 4.16 shows a PEEL spectrum from an alumina grain. This result agrees well with published results for alumina and silica, as seen in Figures 4.17a and 4.17b respectively. It may be recalled that the Si- $L_{2,3}$  edge overlaps with the post edge features of the Al- $L_{2,3}$  edge. In all regions where EDXS showed the presence of silicon, the PEEL spectra revealed a peak at ~107eV which is most likely associated with the Si-  $L_{2,3}$  edge, as shown in Figure 4.18. The spectra from the centers of the triple junctions were also compared to previously published PEELS data and this also suggested the presence of mullite (Kleebe et al. 1996) (see Figure 4.19). In Figure 4.18, the indicated peaks and positions correspond well with the reference spectrum, Figure 4.19. Thus, the bonding environment Si in the triple junction is similar to that of mullite, an aluminosilicate.

In addition to the Al- $L_{2,3}$  edge and Si- $L_{2,3}$  edge a series of Si-K edge PEEL spectra were taken from the center of the triple junction to an adjoining grain boundary, see Figure 4.20. The PEEL spectra were collected near the positions where the EDX spectra were acquired, see Figure 4.10. It may be seen that the spectrum from the triple junction is characterized by two edges, one at 1839 eV and the other at 1846 eV (A and B in Figure 4.20). All the spectra from the grain boundary exhibited an edge at 1846 eV only. Figure 4.20 also has the reference spectrum for  $\text{SiO}_2$ . As the triple junction spectra show, there is an edge at 1839 eV which corresponds to the same position as the Si-K in

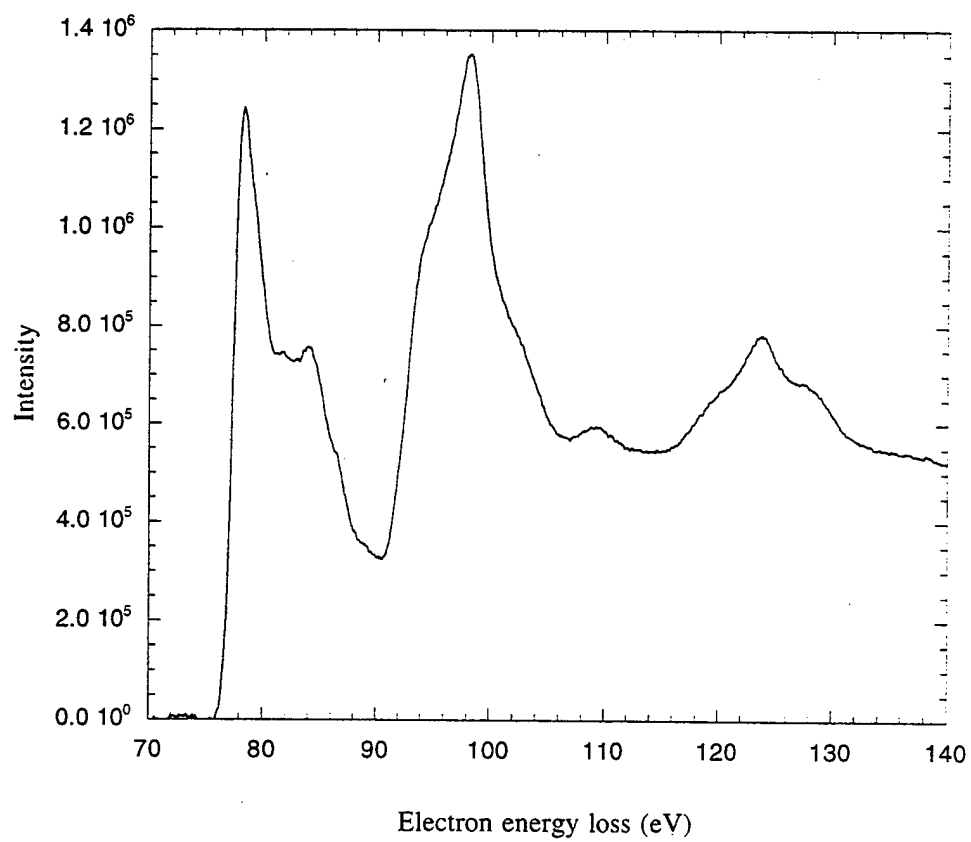


Figure 4.16 PEELS spectra from an alumina grain interior.

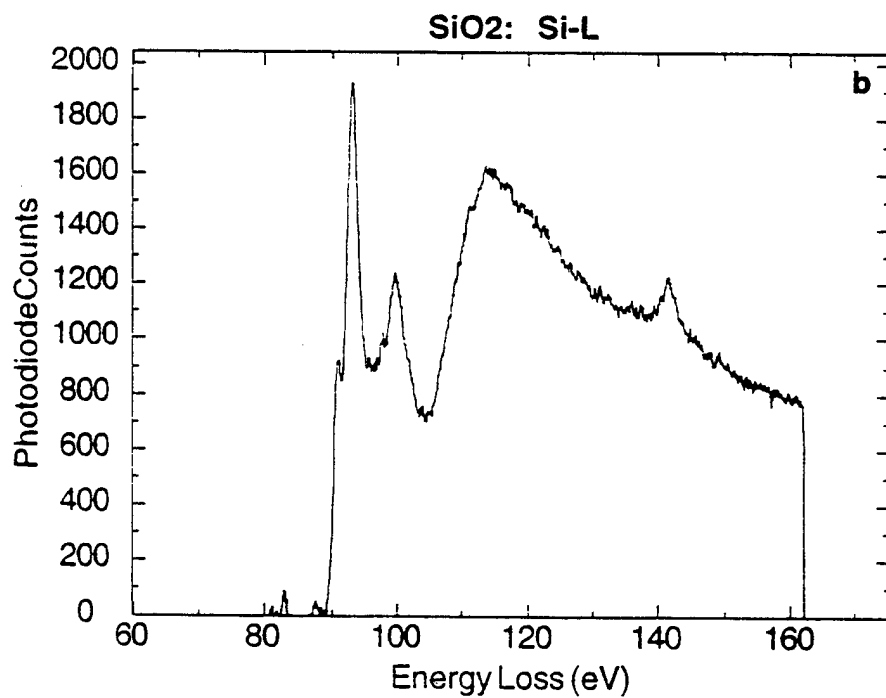
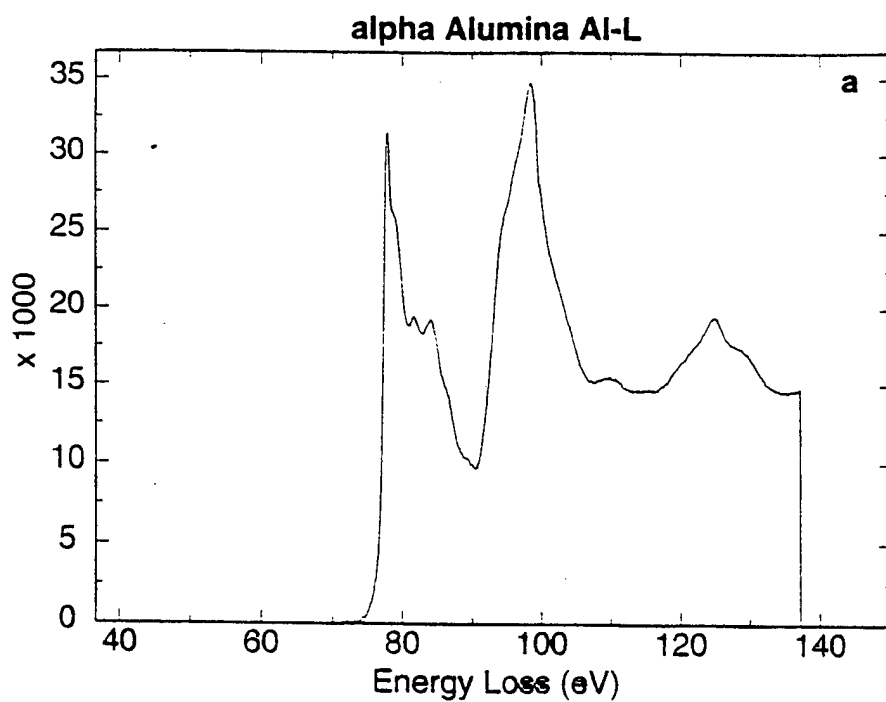


Figure 4.17 Reference PEEL spectra from alumina (a) and SiO<sub>2</sub> (b) (after Kaneko 1997).

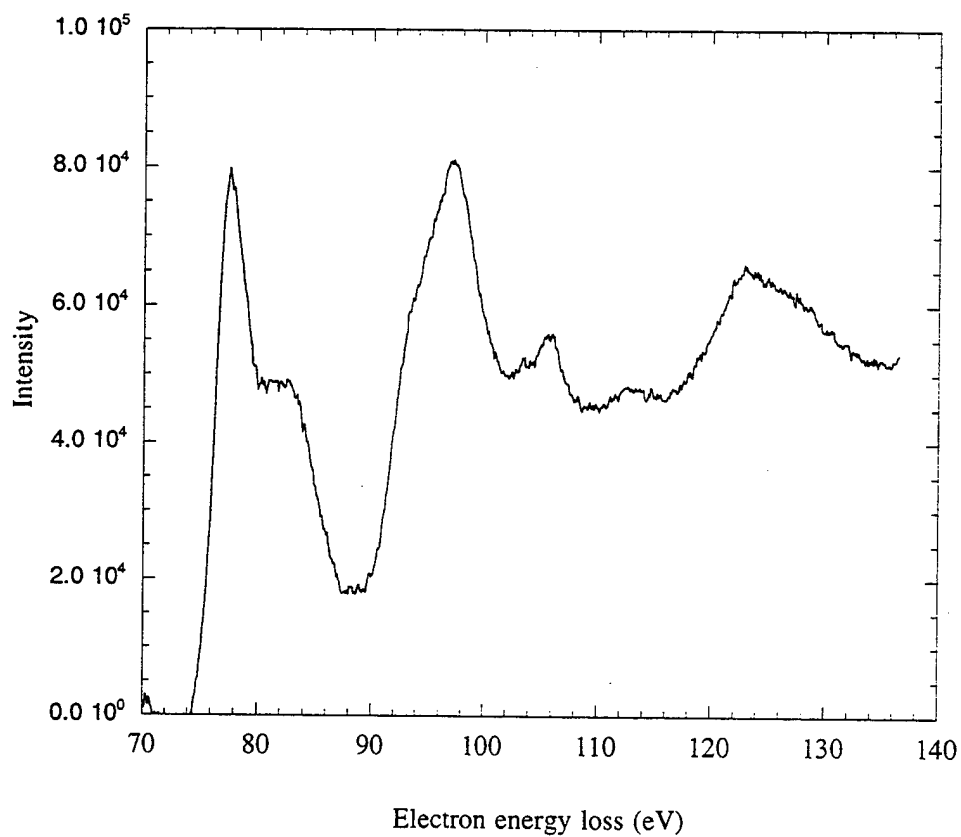


Figure 4.18 PEEL spectrum from the middle of a triple junction. Note the feature at  $\sim 107\text{eV}$ .

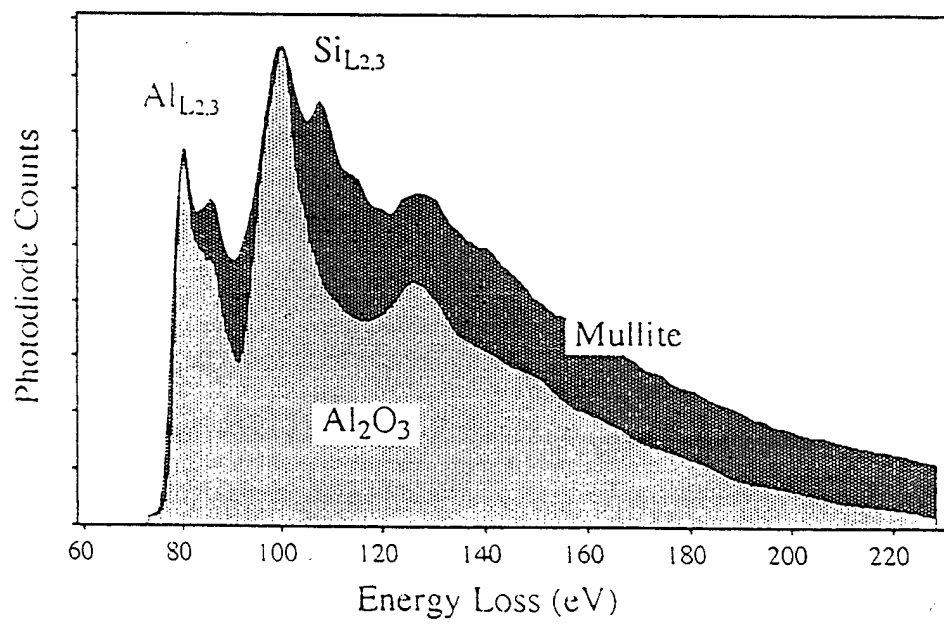


Figure 4.19 Reference PEEL spectra for mullite and alumina (Kleebe 1996).

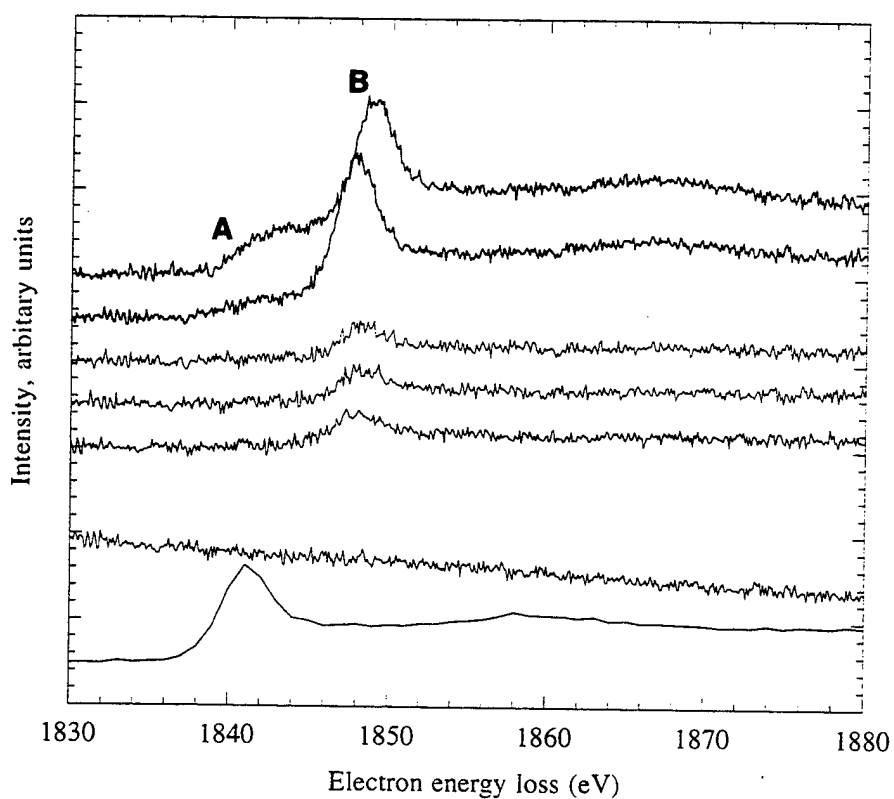


Figure 4.20 PEEL spectra overlays of the Si-K edge from the center of the triple junction (top two spectra) along one of the adjoining grain boundaries (curves shown progressively lower). Spectra from pure  $\text{SiO}_2$  is shown in the bottom-most curve.



the  $\text{SiO}_2$  reference spectrum. The second edge in the spectra (B, Figure 4.20) at 1846 eV corresponds to the same edge position as those found for spectra taken from the grain boundary regions containing Si. Unfortunately, a reference Si-K edge spectrum from single phase mullite could not be found in the literature but it would be reasonable to assume, considering the discussion above, that the Si-K edge occurring at 1846 eV is associated with the component of the spectrum arising from mullite.

The Al-K edge from the triple junction and from the interior of alumina grain are compared in Figure 4.21. Although there is no change in the position of the edge onset, the relative heights of the features marked "a" and "b" show a significant change. In addition, the feature marked "c" appears to have shifted to lower energy loss in the spectra from the triple junction. These changes are most certainly associated with the interactions of the alumina with the silica in the triple junction.

Since the Si-K edge intensity is proportional to the number of Si atoms, the integrated intensity under a 20 eV window was used to determine the variation of Si from the triple junction along the grain boundary. A plot of the integrated intensity versus distance is shown in Figure 4.22. This plot shows that silicon is present in large amounts in the center of the triple junction and decreases with further distance along the adjoining grain boundary. This result agrees well with EDXS results presented earlier.

#### **4. Summary of results from alumina substrate**

Combining the TEM, EDXS and PEELS results with the phase diagram, we conclude that the triple junctions were composed of a mixture of mullite and a glassy,

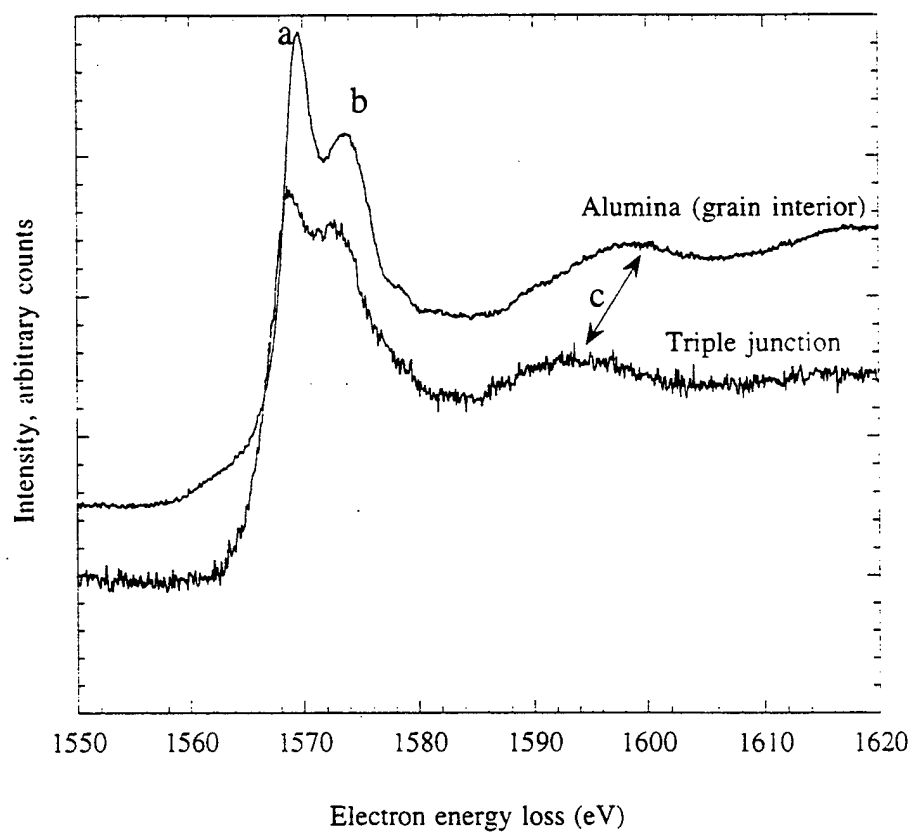


Figure 4. 21 PEEL spectrum of an Al-K edge from the triple junction compared to that of pure alumina.

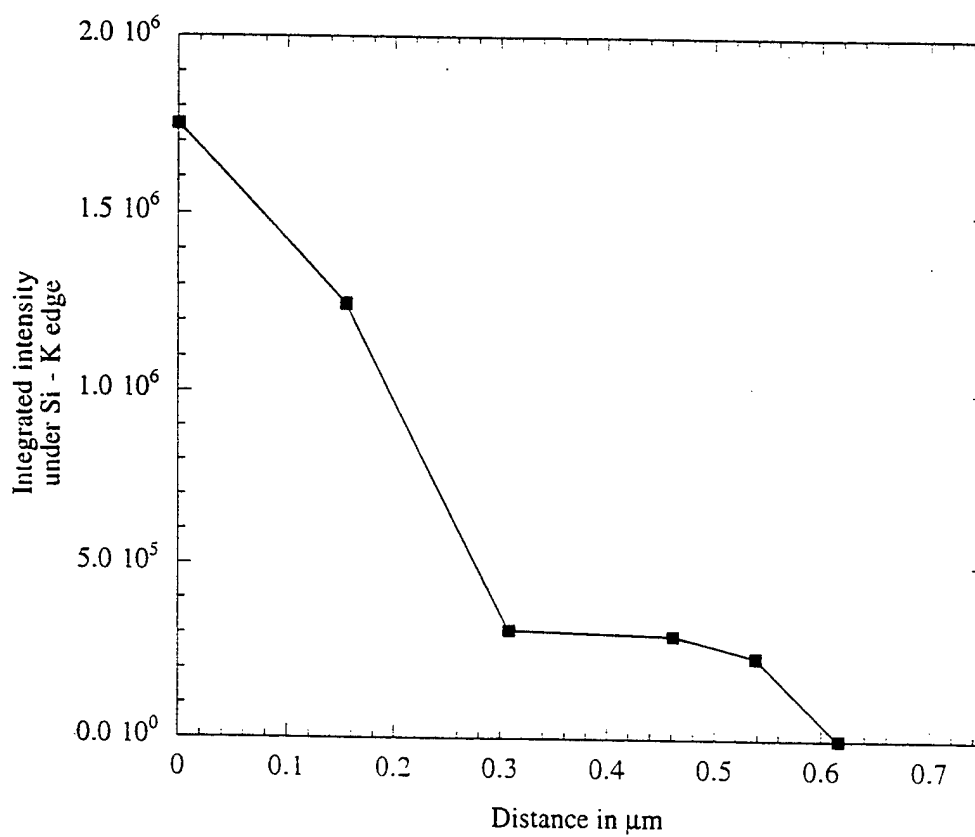


Figure 4.22 Si-K edge intensity versus distance away from the center of the triple junction along an adjoining alumina grain boundary.

silica-rich phase. Si was found in the highest concentrations in the center of the triple junctions and decreased along the adjoining  $\text{Al}_2\text{O}_3$  grain boundaries. In addition, Si at the adjoining triple junction grain boundaries showed coordination similar to that of mullite.

## **B. THE COPPER-ALUMINA INTERFACE**

### **1. Imaging**

Conventional TEM images as well as energy filtered did not reveal contrast variations other than that from the Cu and the  $\text{Al}_2\text{O}_3$  that would indicate a phase at the interface. In addition no voids were observed. Figure 4.23 shows a zero loss energy filtered image of the copper-alumina interface. The difficulty in imaging a possible silica-containing phase at the interface can be attributed to the fact that alumina and silica have the same molecular weights, which means low contrast conditions between the two phases especially if one or both is amorphous as would perhaps be expected for the  $\text{SiO}_2$ . Indeed, diffraction patterns taken from the interface only indicated copper and alumina.

### **2. EDXS**

As in the alumina substrate analysis, EDXS was used to determine the presence and distribution of impurities along the Cu- $\text{Al}_2\text{O}_3$  interface. EDX spectra from the Cu grains showed no  $\text{Al}_2\text{O}_3$  or impurities. No Si or Al was found in the bulk Cu that formed the interface, see Figures 4.24. There was no Cu or Si detected in the bulk alumina. Thus, it appears that no interdiffusion occurred during the high temperature bonding process.

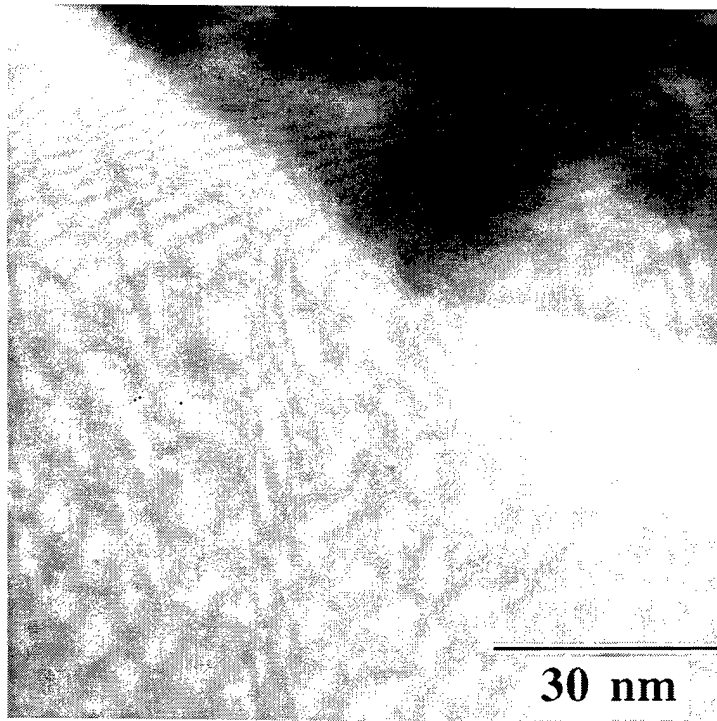


Figure 4.23 Zero-loss energy filtered image of the copper-alumina interface.

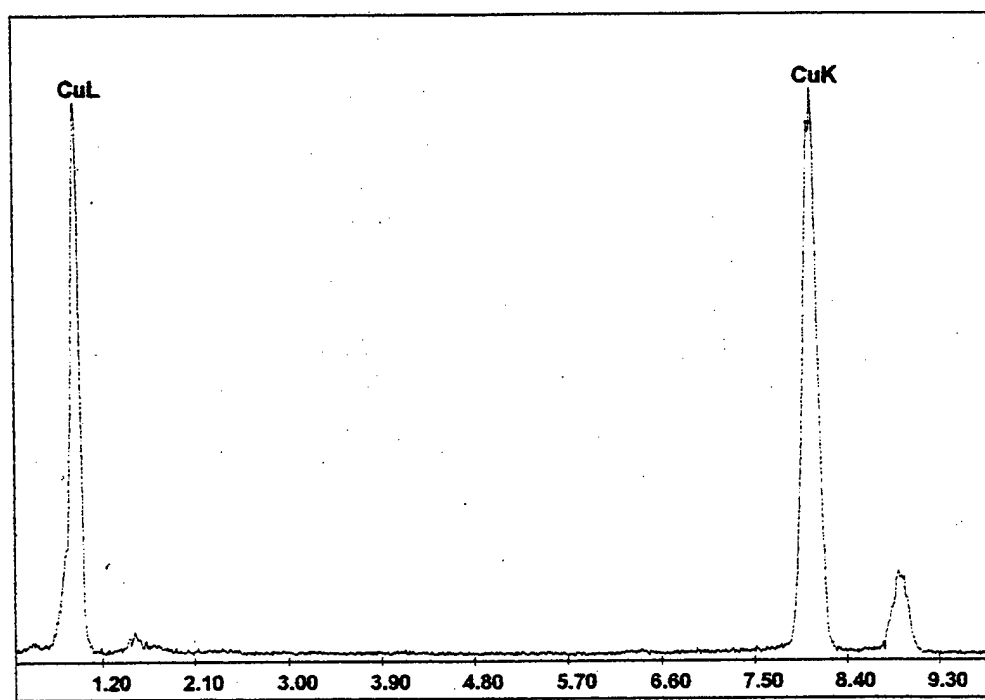


Figure 4.24 EDX spectrum from a copper grain interior.

Figure 4.25 shows ZAF corrected analysis from a typical interface region for 100 nm thickness and 150 nm thickness. In Figure 4.25 the ZAF corrections were calculated with an average density of Cu and  $\text{Al}_2\text{O}_3$ . Again, analysis for variance due to density and thickness variations in ZAF inputs accounts for  $\pm 0.6$  at. % variation in composition.

Although conventional microscopy and diffraction showed no interface phases, silicon was detected using EDXS. EDX spectra taken at several locations along the interface showed that silicon was present in varying amounts. In some regions there was no detectable amounts of Si. Figure 4.26 shows EDX spectra from a region with varying amounts of silicon and Figure 4.27 shows one where Si is absent. Detectable amounts of silicon were found to exist over large distances along the interface,  $>1 \mu\text{m}$  away from the intersection of the alumina grain boundary and the copper-alumina interface. As mentioned earlier the Si distribution was non-uniform. Figures 4.28 show the quantitative EDXS analysis for the spectra shown in Figure 4.26. EDXS analysis from many locations on the copper-alumina interface showed the silicon concentration to vary from  $1.0 \pm 0.5$  at.% to  $10.0 \pm 0.5$  at.% along the interface.

### 3. PEELS

Energy filtered images were taken in an attempt to image possible interface phase(s). Figure 4.29 shows the zero loss (inelastically filtered) image of a region of interface. Figure 4.30 is a Si-K jump ratio image from the boxed region shown in Figure 4.29. The jump ratio image shows that Si is present at the interface. Figure 4.31 shows a line profile taken from the box indicated in Figure 4.30. The line profile shows the

A:\HASH10.SPC Label :

Foil thickness = 100 nm

kV : 200.00      X Tilt : 10.00      Y Tilt : 0.00      Azimuth : 0.00

Elevation : 17.60    Tc : 40

Detector Type : SUTW    Resolution : 138.73    Lsec : 170

Thin Apx, Abs Corr

Theoretical KAB, Elements, Model : Zaluzec□□

Element	Weight %	Atomic %	Xpt
O K	28.0	48.7	0.931
AlK	32.8	33.8	0.499
SiK	0.6	0.6	0.539
CuK	38.6	16.9	0.008
Total	100.0	100.0	

Inc Angle = 30.00    Abs Path = 318.85

Density = 6.45    Iter = 3

Element	Net Inte.	Bkgd Inte.	Inte. Error	P/B
O K	15.82	0.71	1.97	22.41
AlK	58.90	0.94	1.01	62.58
SiK	0.39	0.97	11.77	0.92
CuK	41.64	0.19	1.19	221.19

A:\HASH10.SPC Label :

Foil thickness = 150 nm

kV : 200.00      X Tilt : 10.00      Y Tilt : 0.00      Azimuth : 0.00

Elevation : 17.60    Tc : 40

Detector Type : SUTW    Resolution : 138.73    Lsec : 170

Thin Apx, Abs Corr

Theoretical KAB, Elements, Model : Zaluzec□□

Element	Weight %	Atomic %	Xpt
O K	26.1	46.6	0.631
AlK	32.4	34.4	0.343
SiK	0.6	0.6	0.365
CuK	40.9	18.4	0.006
Total	100.0	100.0	

Inc Angle = 30.00    Abs Path = 212.57

Density = 6.45    Iter = 3

Figure 4.25 ZAF corrected EDXS results from the interface using 100 nm and 150 nm thicknesses with an average density of copper and alumina.



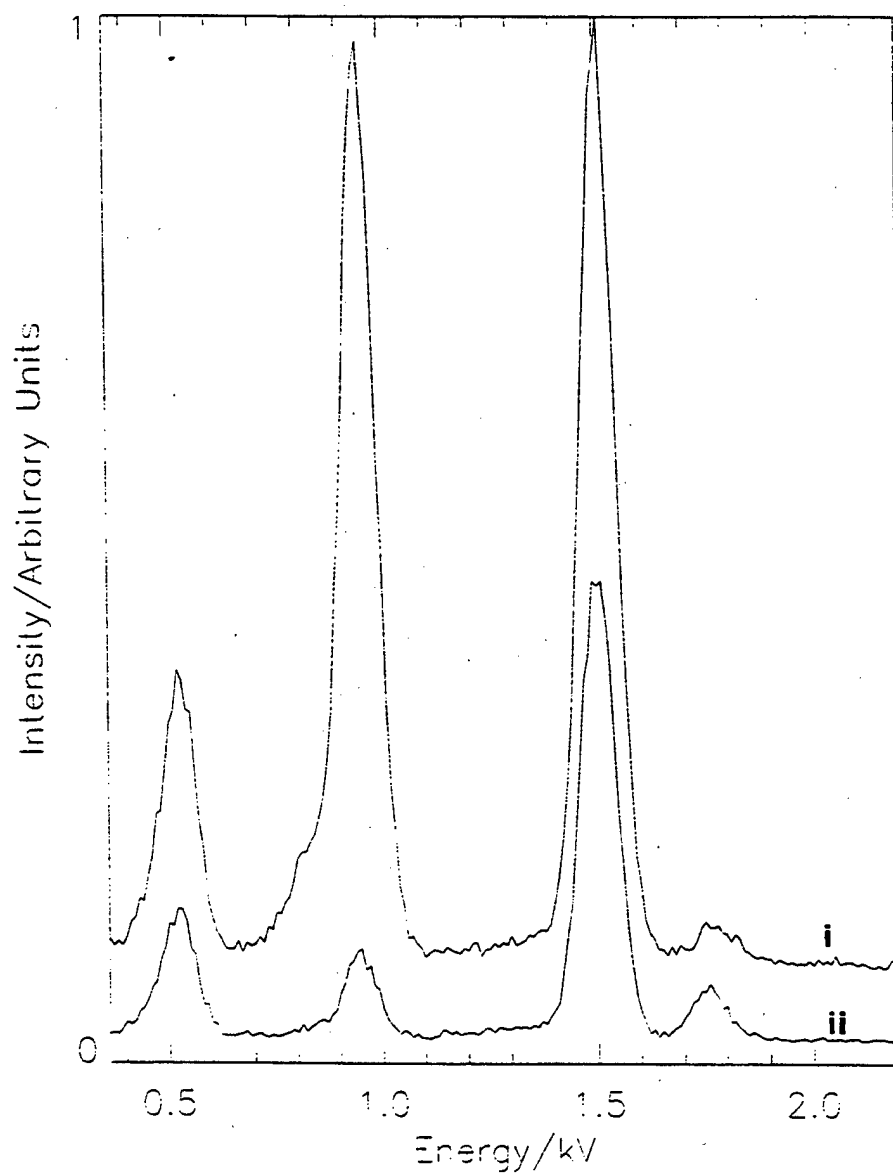


Figure 4.26 EDX spectra from the interface (i) low Si concentration and (ii) high Si concentration.

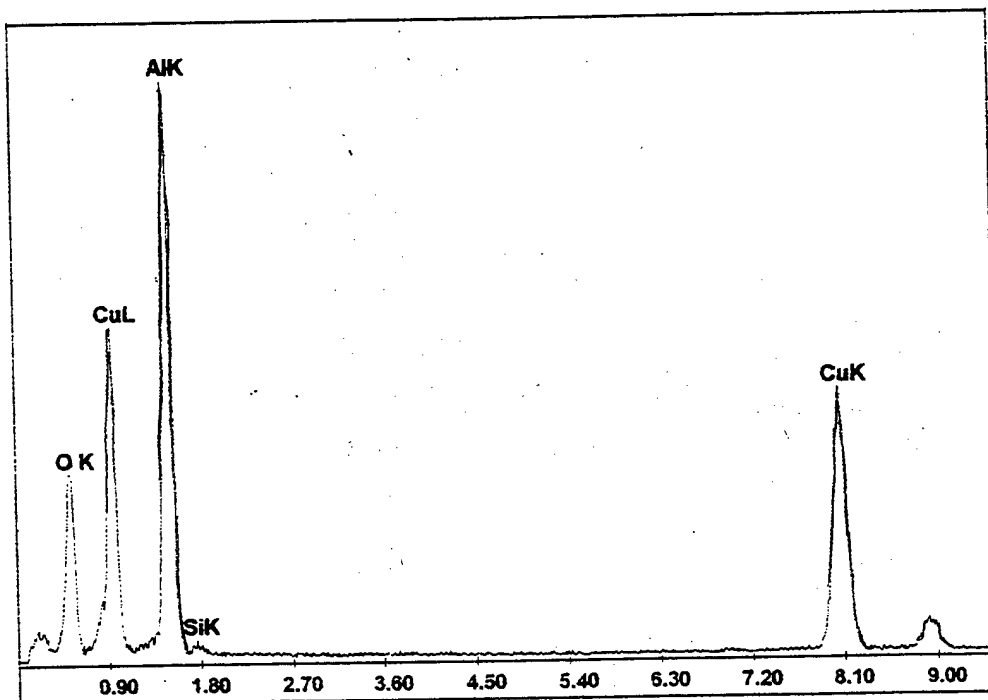


Figure 4.27 EDX spectrum from an interface region that has very little Si present.

### Low Si

Element	Weight %	Atomic %	Xpt	Foil thickness = 100 nm
O K	18.3	38.6	0.671	
AlK	24.0	30.0	0.425	
SiK	1.1	1.3	0.386	
CuK	56.6	30.1	0.006	
Total	100.0	100.0		

Element	Weight %	Atomic %	Xpt	Foil thickness = 150 nm
O K	20.0	40.8	0.993	
AlK	24.9	30.1	0.618	
SiK	1.2	1.3	0.571	
CuK	54.0	27.7	0.009	
Total	100.0	100.0		

Inc Angle = 90.00 Abs Path = 318.85  
Density = 6.45 Iter = 3

### High Si

Element	Weight %	Atomic %	Xpt	Foil thickness = 100 nm
O K	29.3	46.2	0.642	
AlK	42.0	39.4	0.240	
SiK	6.0	5.4	0.335	
CuK	22.7	9.0	0.005	
Total	100.0	100.0		

Inc Angle = 90.00 Abs Path = 212.57  
Density = 6.45 Iter = 3

Element	Weight %	Atomic %	Xpt	Foil thickness = 150 nm
O K	31.2	48.3	0.945	
AlK	41.5	38.1	0.352	
SiK	6.0	5.3	0.493	
CuK	21.3	8.3	0.008	
Total	100.0	100.0		

Figure 4.28 ZAF corrected EDXS results for the high and low Si regions along the interface.

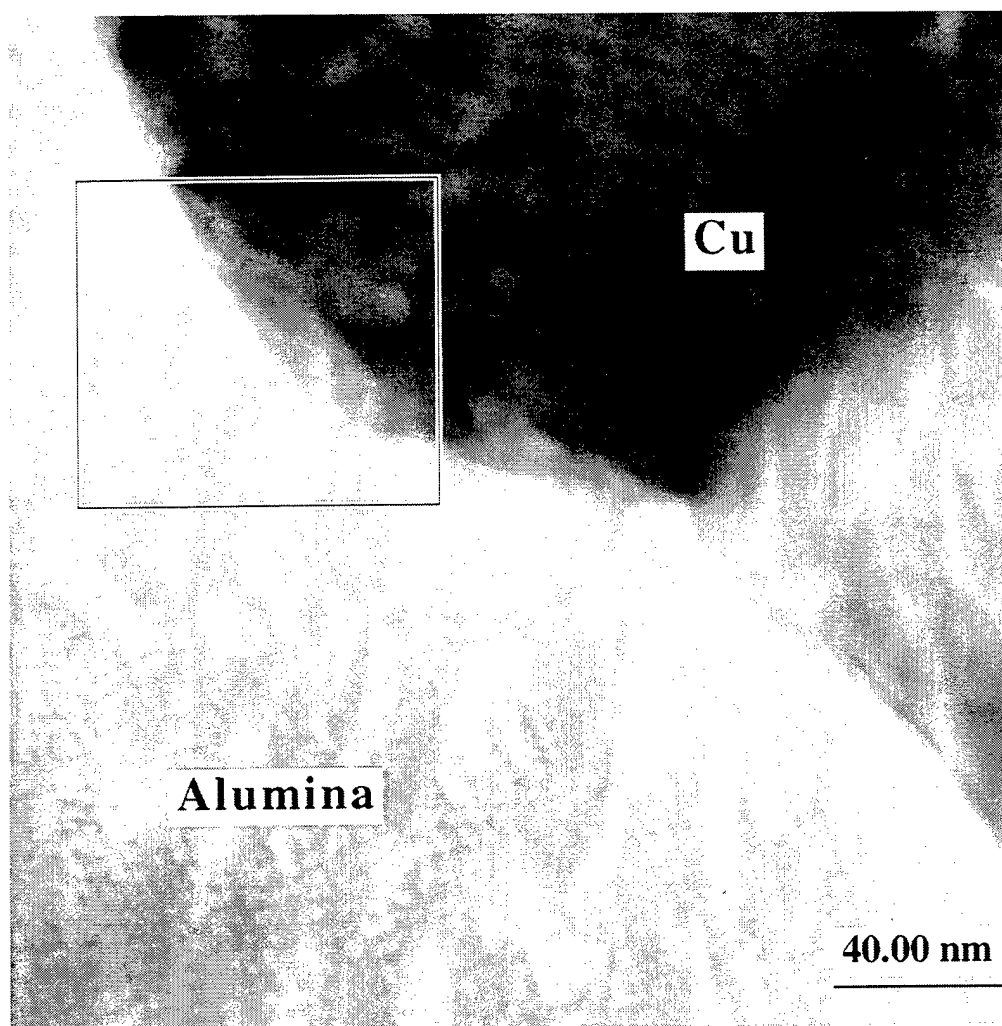


Figure 4.29 Zero-loss energy filtered image of the copper-alumina interface.

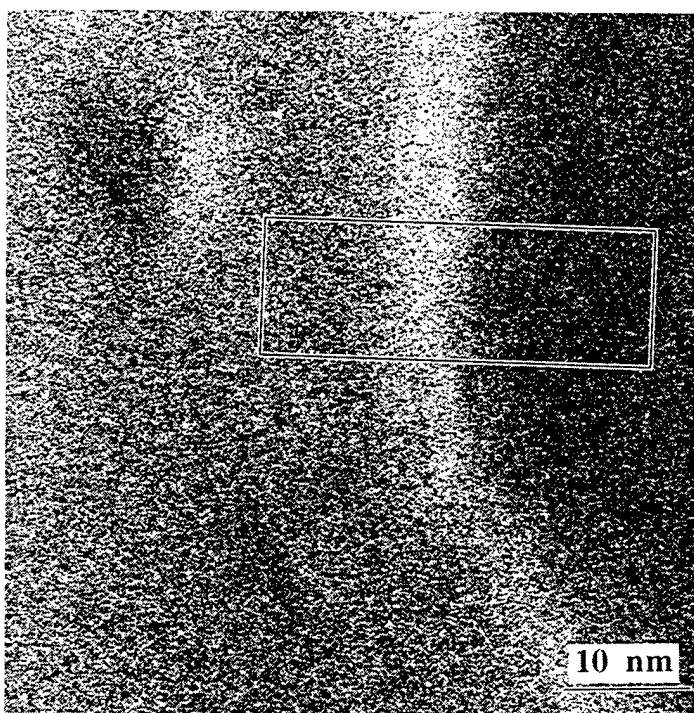


Figure 4.30 Si-K jump ratio image from the box indicated in Figure 4.29.

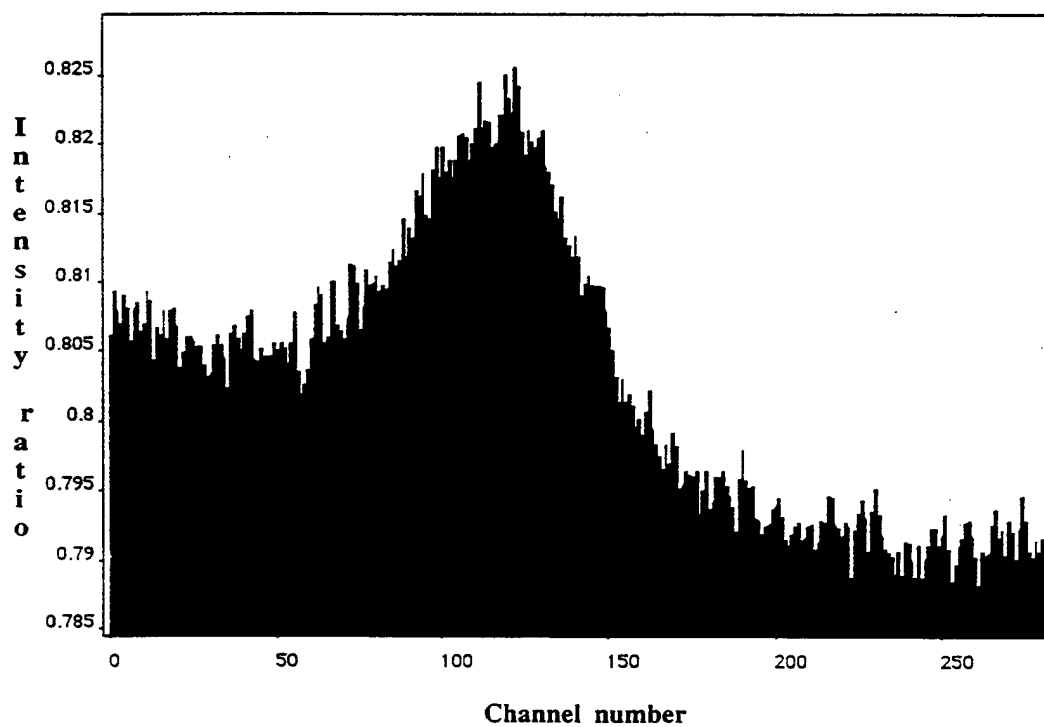


Figure 4.31 Line profile from the box indicated in Figure 4.30.

integrated intensity for Si-K edge. As Figure 4.31 shows, there is Si enrichment along the metal-ceramic interface. Although there is clear evidence from the Si-K jump ratio map and the Si-K intensity line profile that Si is present at the interface, neither the number of Si atoms nor the width of the Si-rich region could be established for three reasons. Firstly, the interface may not have been perfectly aligned with the electron beam. Secondly, the sample thickness may have varied across the region of analysis. There is evidence for this since the line profile is slightly sloped in Figure 4.30. Thirdly, it is very difficult to focus PEEL Si-K images because they occur at the high energy loss (around 1839 eV). Thus, the width of the observed Si rich region in Figure 4.30 may be exaggerated. Nonetheless, PEEL images show that Si is present at the interface, which agrees well with the EDXS results.

PEEL spectra were taken to determine the chemical coordination of the copper, aluminum, silicon and oxygen at the interface. All PEEL spectra were acquired at 0.1eV energy dispersion.

A series of spectra were collected in the 50eV to 150eV range which includes the Al-L<sub>2,3</sub>, Cu-M<sub>2,3</sub> and Si-L<sub>2,3</sub> edges. Three distinct PEEL spectra types were obtained from the interface. The first two types of spectra came from areas in which EDXS analysis showed silicon. These spectra were characterized by a significant feature at ~107eV. This feature is attributed to the Si-L<sub>2,3</sub> edge. The PEEL spectra were categorized into high and low silicon regions. Figure 4.32 shows an overlay of typical high and low silicon regions PEEL spectra. The third type of spectra did not have the ~107 eV feature, as seen in Figure 4.33.

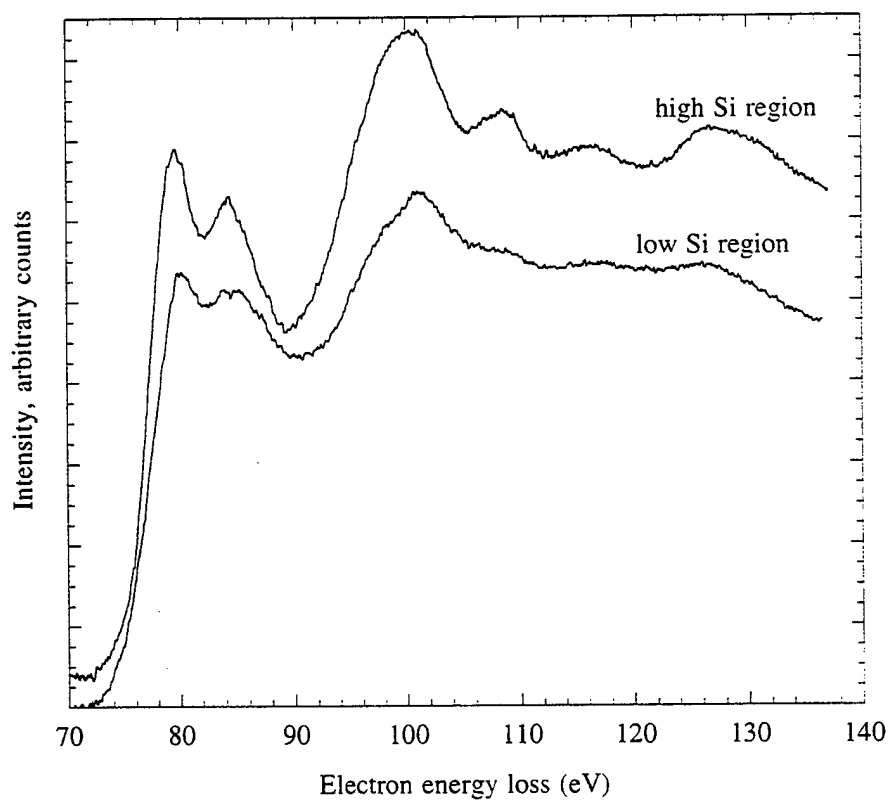


Figure 4.32 Overlay of PEEL spectra from high and low Si regions at the metal-ceramic interface.



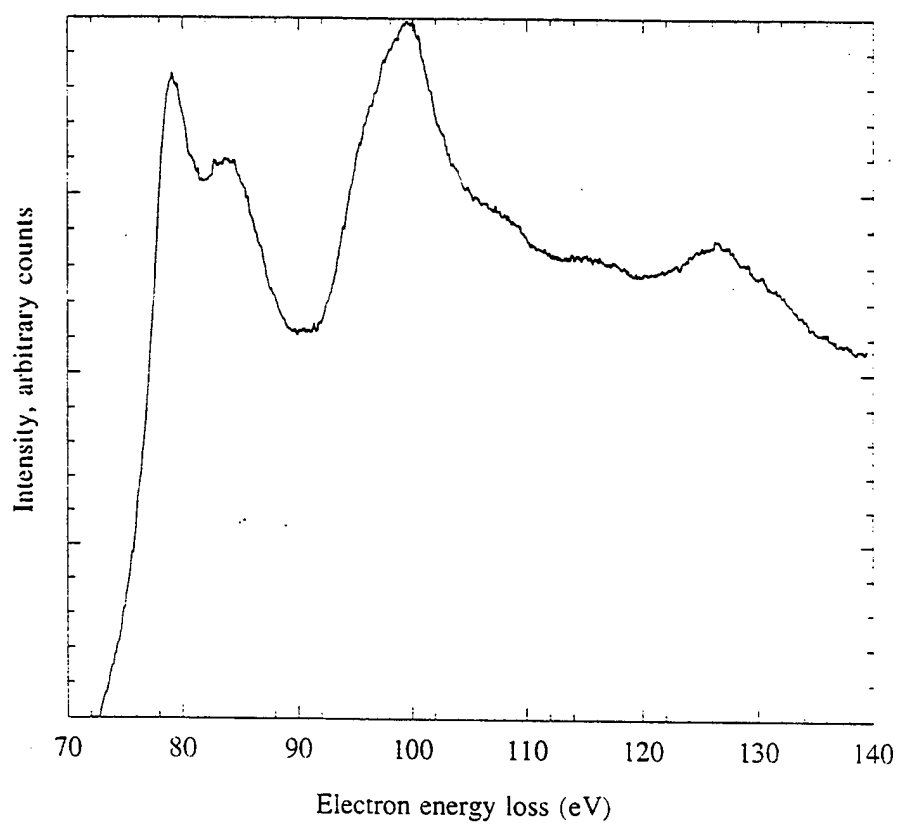


Figure 4.33 PEEL spectrum from a region in which there was very little Si at the metal-ceramic interface.

In order to determine the coordination effects at the interface, the spatial difference technique was applied to the three spectrum types. The spatial difference technique was applied using the guidelines set by Brydson (1993). In all cases appropriate fractions of Cu-M<sub>2,3</sub> edge (from Cu) and Al-L<sub>2,3</sub> edge (from Al<sub>2</sub>O<sub>3</sub>) were subtracted from the acquired interface spectra. Examples of the reference spectra for the Cu-M<sub>2,3</sub> edge and Al-L<sub>2,3</sub> edge are given in Figure 4.34 along with an interface spectrum. The resulting spatial difference spectrum is shown in 4.35. As seen in Figure 4.35, the residual spectrum from Si free regions (as indicated by EDXS and PEELS) shows coordination effects that are similar in nature to metal-to-metal coordination (Brydson et al. 1995 and Müllejans and Bruley 1995). In Figure 4.36 residual spectra from the high and low silicon regions show the presence of a feature at ~107 eV. The residual spectra from Si enriched areas show that the segregation of Si introduces distinct chemical environment changes at the copper-alumina interface. Thus, there are two distinct residuals that correlate to the presence and absence of Si at the interface.

Comparison of the spatial difference spectrum from the silicon-rich interface to the spectrum from the center of the triple junction showed identical features, as marked by arrows in Figure 4.37. Recalling that the spectrum from the triple junction was similar to that of mullite, Figure 4.19, we can conclude that the atomic environments near the Si enriched copper-alumina interface regions are similar to that of an aluminosilicate like mullite. However, sufficient information to unambiguously identify the nature of chemical bonding was not present, since similar atom coordination could arise in many ways.

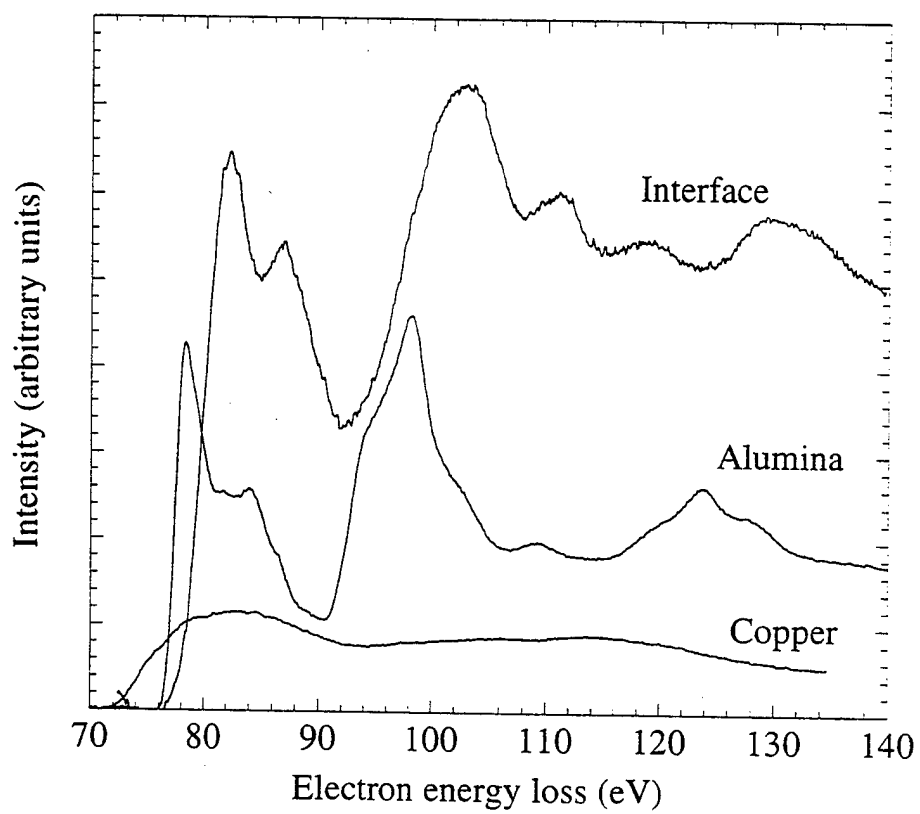


Figure 4.34 Overlay of PEEL spectra from the interface, alumina (Al-K), and copper (Cu-M).

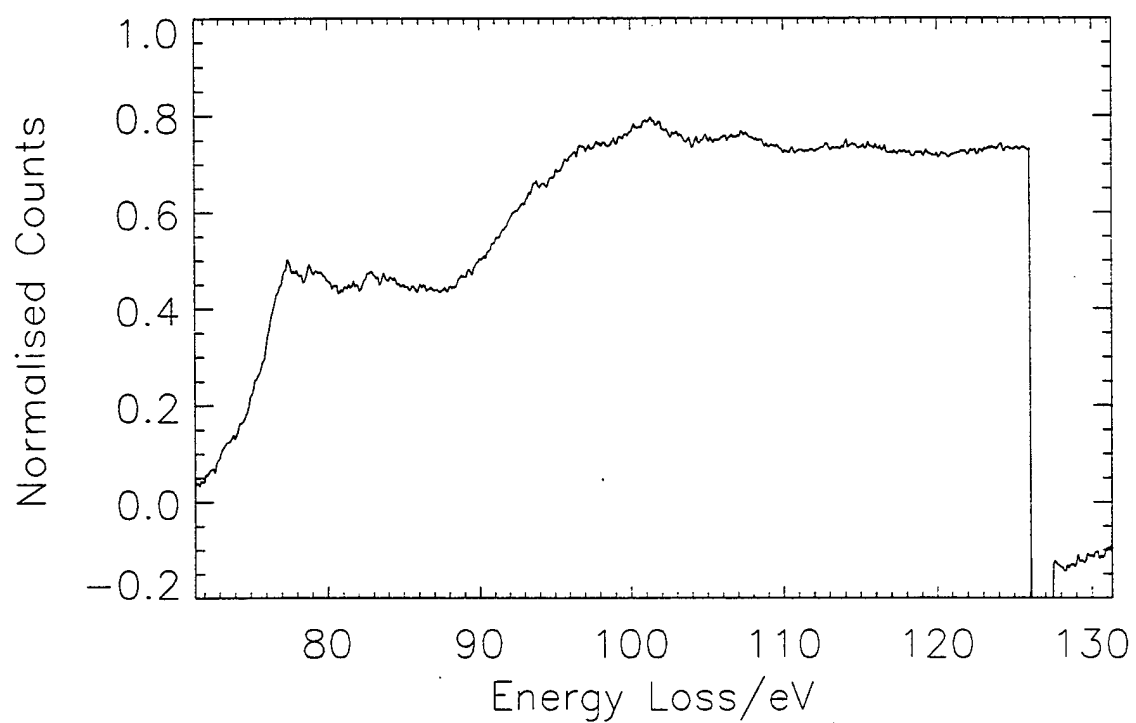


Figure 4.35 Spatial difference residual spectrum from the spectra shown in Figure 4.34.

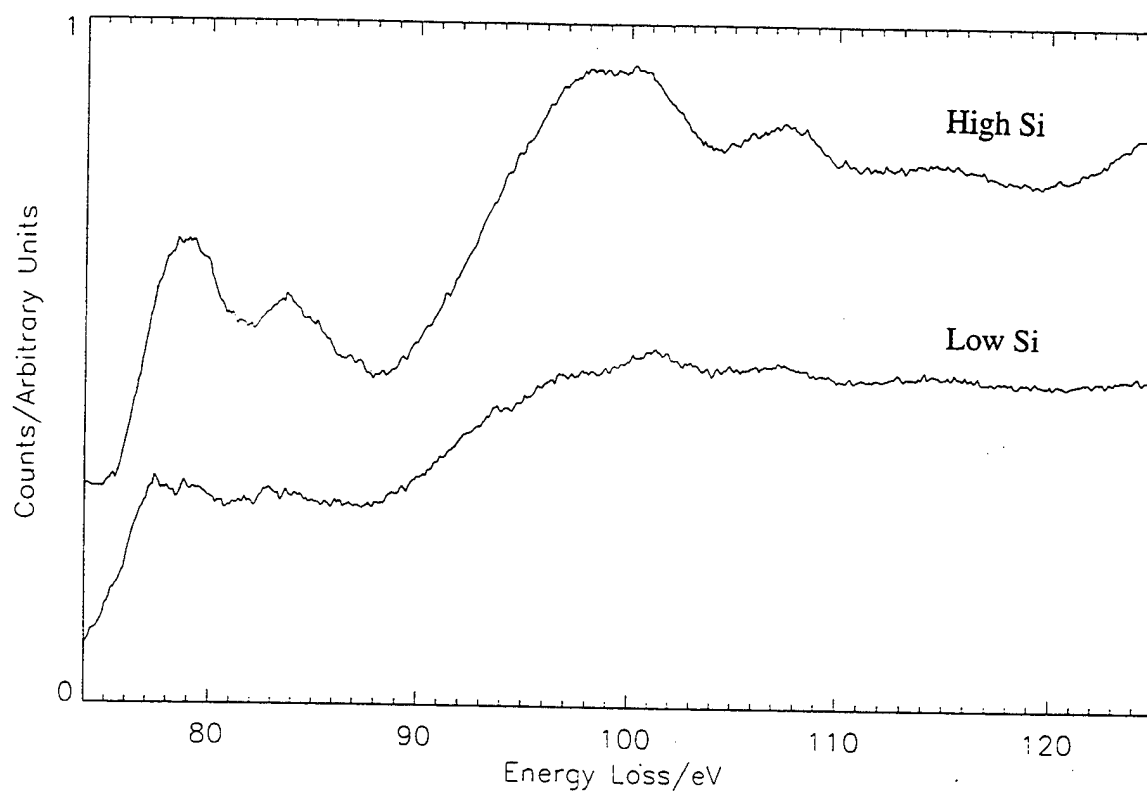


Figure 4.36 Spatial difference residual spectra from high and low Si regions at the interface.

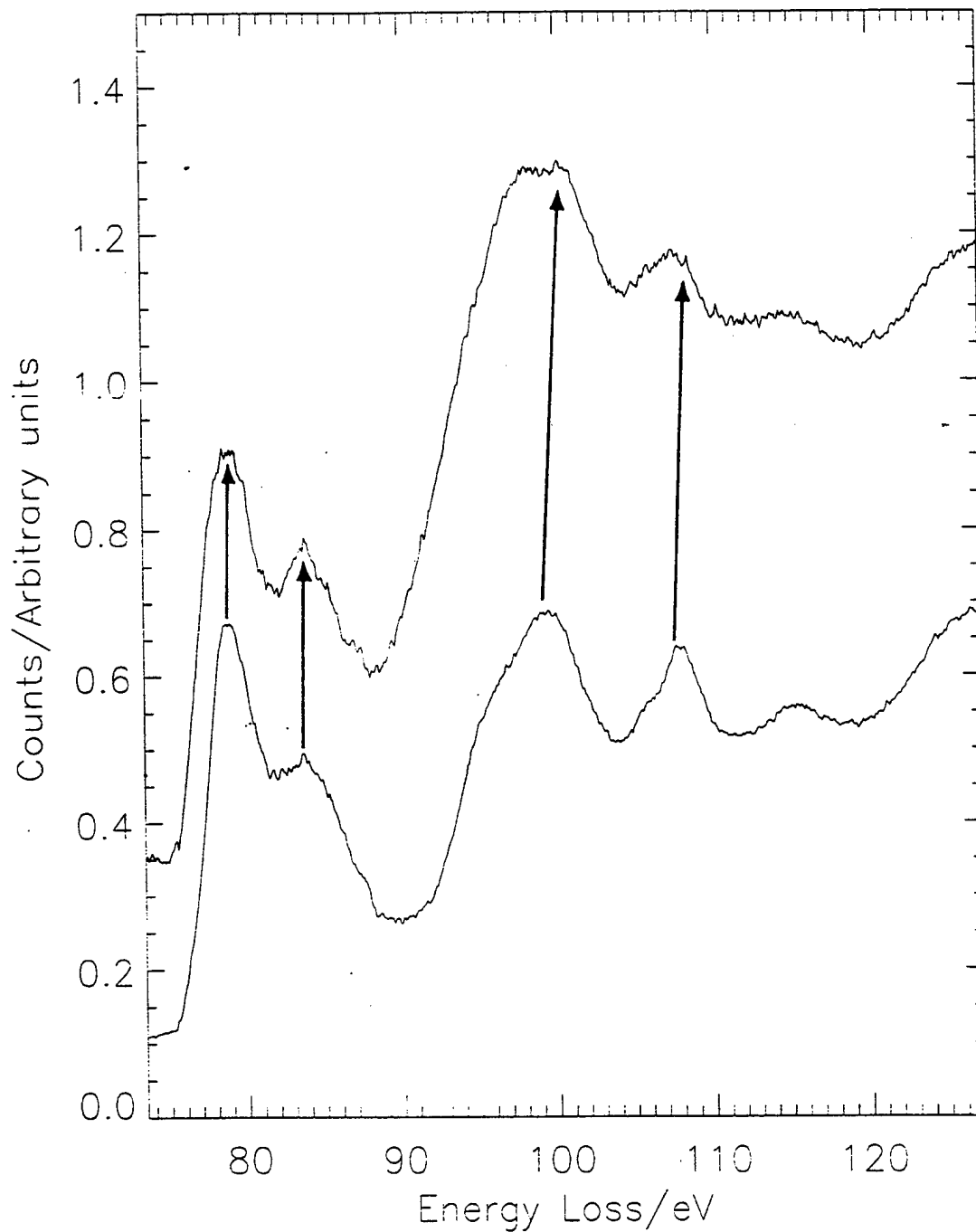


Figure 4.37 Comparison of the spatial difference residual spectrum from a Si-rich region at the interface (upper curve) and the PEEL spectrum from the triple junction (lower curve).

The O-K edges, Cu-K edges and Si-K edges in the PEEL spectra were also examined. Figure 4.38 shows the O-K edge from spectra taken from an alumina grain interior, the interface and an alumina triple junction. As seen in this Figure, there is pre-edge feature marked "a", which may be attributed to beam damage in the spectra from alumina as well as the interface (Kaneko, private communication, 1997). Noticeably this feature is absent in the spectrum from the triple junction; presumably due to the stabilization of the alumina by silica against electron beam damage. The O-K edge, marked "b" in Figure 4.38, and associated features, marked "c" and "d", are present in all these three spectra. However, the ratio of features, marked "c" and "d", Figure 4.38, change in the triple junction compared to those given in the alumina grain interior or the interface. Comparison of the spectrum from  $\text{Al}_2\text{O}_3$  agrees well with published data for  $\alpha$ -alumina with respect to number of features and their relative intensity ratios, Figure 4.39.

The Cu-L<sub>2,3</sub> edge from the interface and from the Cu grain interior are compared in Figure 4.40 and they appear to be the same, exhibiting no chemical change. The absence of white lines (sharp intensity at 931 eV and 951 eV) in these spectra indicates that copper oxide is not present (Menon and Krishnan 1992). Thus, copper is not as chemically active as Al, Si, or O appear to be under the diffusion bonding conditions adopted in the present work.

Although Si-K jump ratio maps were generated, high energy ( > 1000 eV) loss spectra of trace elements usually have low signal to noise ratio. As a consequence, the Si-K edge (1839 eV) spectra from the interface were found to be difficult to quantify and to study for fine structure.

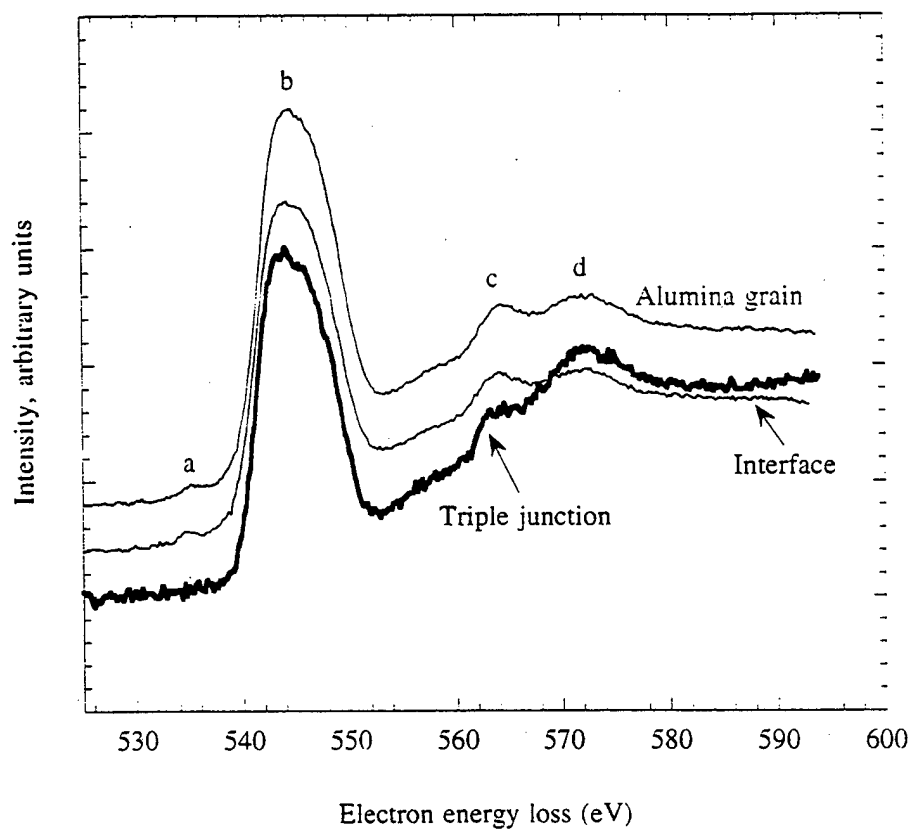


Figure 4.38 Overlay of the PEEL spectra from an alumina grain, the interface, and a triple junction.



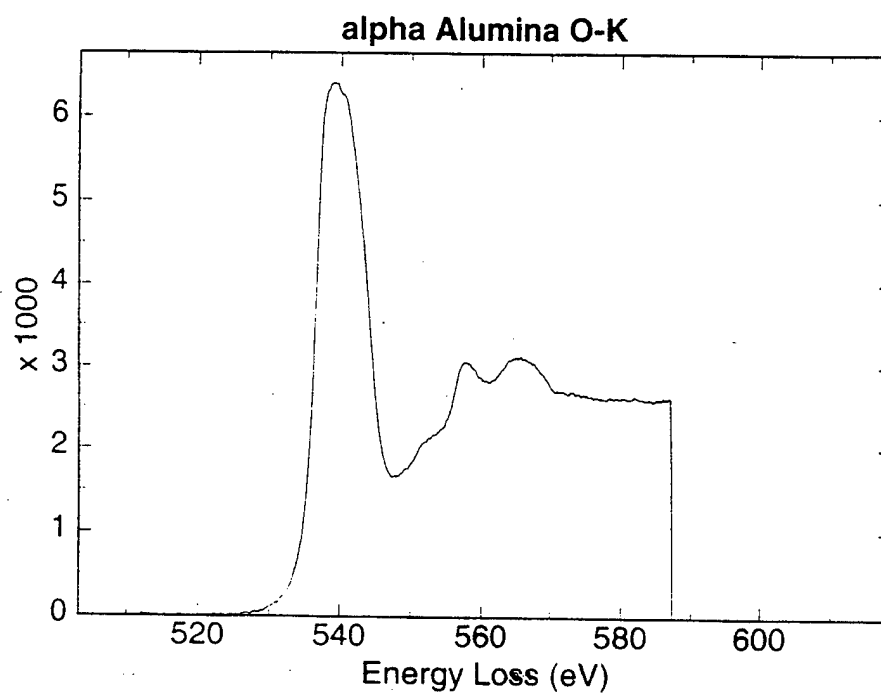


Figure 4.39 Reference PEEL spectrum for O-K edge in alumina (Kaneko 1997).

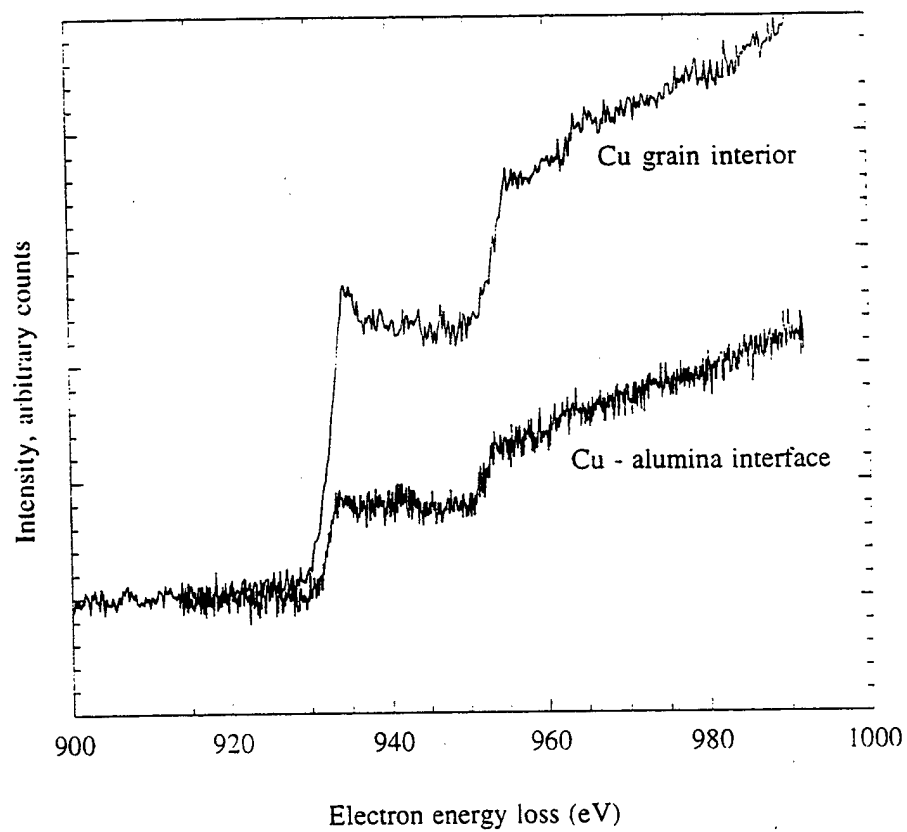


Figure 4.40 Overlay of PEEL spectra of the O-K edge in copper and at the copper-alumina interface.

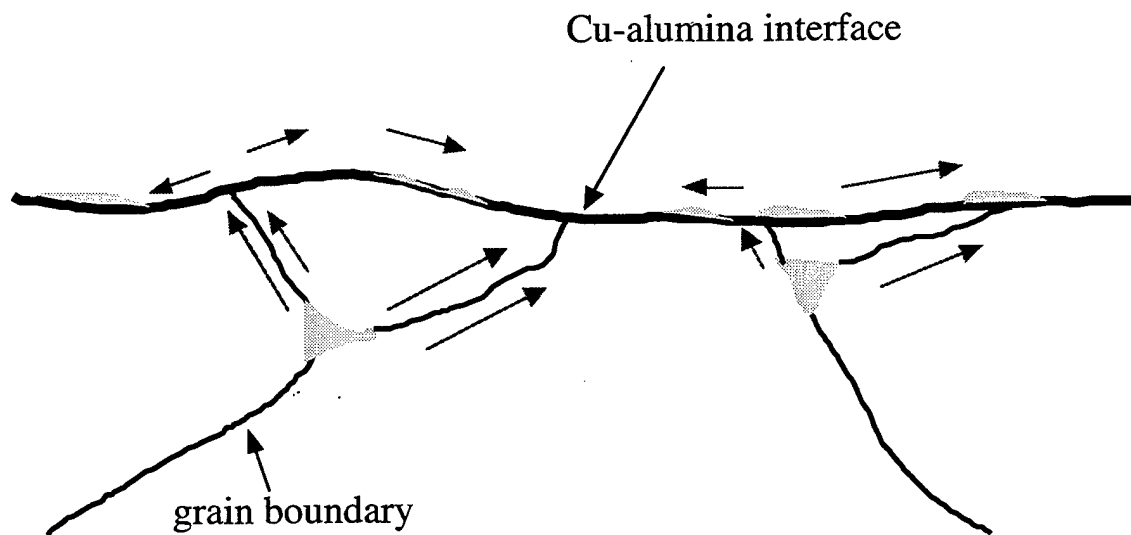
#### **4. Summary of results from copper-alumina interface**

The presence of silicon at the copper-alumina interface studied in the present work can be described by two scenarios both of which are supported by the data. This is best described by means of the schematic shown in Figure 4.41. The first case is that the interface was close to a triple junction or Si enriched grain boundary, see Figure 4.41. This case is statistically probable given the Cu grain size, 20  $\mu\text{m}$ , versus alumina grain size, 1.0 to 5.0  $\mu\text{m}$ . The second case is that silicon diffused along the grain boundary from a nearby triple junction to the interface, also seen in Figure 4.41. The varying concentrations of Si along the interface may be associated with the proximity of the interface to Si enriched triple junctions and grain boundaries in the bulk alumina. It is evident that silicon can diffuse via the grain boundaries from the bulk alumina to the interface. Since silicon was detected over large distances,  $> 1.0 \mu\text{m}$ , away from the intersection of the alumina grain boundary and the copper alumina interface, it is clear that Si diffused along the interface.

The mere presence of silicon at the copper alumina interface raises several questions as to the contribution of silicon to the strength of the interface. Dalglish et al. (1993) have shown that mechanical tests of copper diffusion bonded to commercial alumina (which has silicon impurities) has higher fracture strengths than copper bonded to sapphire (single crystal, high purity alumina). They also showed that fracture occurred in the ceramic in the polycrystalline case and at the interface for the single crystal case. It was suggested that silica may contribute to the filling of pores at the interface providing increased interface strength (Dalglish 1993). The microstructural data supports this

## COPPER

 Si-rich



## ALUMINA

Figure 4.41 Sketch of the copper-alumina interface and a nearby triple junction and grain boundary.

postulation in that there were no voids seen at the microscopic level. The contribution of silicon to interface strengthening is possible (through void elimination), however it is believed that Si enhances the adhesion of the copper-alumina interface by creating strong chemical bonds between Cu, Al, O and Si. The PEELS results suggest such a situation, but we have not explored the exact nature of these bonds. Such an effort would require extensive high resolution PEELS studies complemented by theoretical modeling, such as multiple scattering calculations.

## **VI CONCLUSIONS**

### **A. ALUMINA TRIPLE JUNCTIONS AND GRAIN BOUNDARIES**

i) Silicon segregates to the triple junctions and the adjoining grain boundaries. These results agree well with other published work, Kingery et al. (1976) and Brydson (1995), on Si segregation in alumina.

ii) A mixture of crystalline mullite and a glassy, silicon rich phase was found at the triple junctions. This conclusion was arrived at by combining SAD, EDXS and PEELS experiments together with information from published alumina-silica phase diagram.

iii) EDXS and PEELS analysis found low concentrations of silicon along grain boundaries near triple junctions. ELNES from PEEL spectra from the alumina grain boundaries containing silicon suggest that the Si in this location has a coordination similar to mullite.

### **B. COPPER-ALUMINA INTERFACES**

i) There was no apparent diffusion of copper into the alumina or aluminum into the copper.

ii) Copper appears to be not as chemically active as Al, Si or O for the particular interface studied.

iii) The TEM studies indicated that no interface phases had formed in these vacuum diffusion bonded samples.

iv) EDX analysis at the interface showed that silicon was present at the metal-ceramic interface in varying concentrations from  $1.0 \pm 0.5$  at.% to  $10.0 \pm 0.5$  at.%.

v) The silicon distribution along the copper-alumina interface was nonuniform. High silicon concentrations produced a significant PEELS peak at  $\sim 107$  eV. Low silicon concentrations also showed a significant feature at  $\sim 107$  eV. When the spatial difference technique was applied to these two types of spectra, we saw spectra that were similar to mullite, an aluminosilicate in the high Si regions. In cases very little or no Si ( $< 0.4$  at. %) as determined by EDXS, the generated spatial difference residual spectrum that showed metal-metal coordinations similar to those reported by Brydson (1995) and others. The residual spectra from the interface areas with high silicon concentration were similar to that obtained from the center of the triple junction; thus leading to the conclusion that the Si present at the interface had an atomic environment similar to that of an aluminosilicate, such as mullite.

vi) These results suggest that Si segregation may contribute to the observed higher strength of the metal-ceramic composite by void filling and improved bonding between the copper and alumina substrate.

## REFERENCES

- Bertaud, C., Courbiere, M., Esnouf, C., Juve, D., and Treheux, D., *Study of Copper-Alumina Bonding*, Journal of Materials Science, 24, pp. 4545-4554, 1989.
- Brydson, R., *Probing the Local Structure and Bonding at Interfaces and Defects using EELS in the TEM*, Journal of Microscopy, Vol. 180, Pt3, pp. 238-249, 1995.
- Brydson, R., Müllejans, H., Bruley, J., Trusty, A. P., Sun, X., Yeomans, J. A., and Rühle M., *Spatially Resolved Electron Energy-Loss Studies of Metal-Ceramic Interfaces in Transition Metal/Alumina Cermets*, Journal of Microscopy, Vol. 177, Pt. 3, March, pp. 369-386, 1995.
- Crispin, R.M. and Nicholas M. G., *Alumina-Copper Diffusion Bonding*, Ceram. Eng. Sci Proc., 10 [11-12], pp. 1575-1581, 1989.
- Davis, R. F. and Pask, J. A., J. Am. Ceram. Soc., 55 [10], pp. 525, 1972.
- Dalgleish, B. J., Saiz E., Tomsia, A.P., Cannon, R. M., and Ritchie, R.O., *Interface formation and Strength in Ceramic-Metal Systems*, Scripta Metallurgica et Materialia, Vol. 31, No. 8, pp. 1109-1114, 1994.
- Dehm, G., Scheu, C., and Rühle M., *Atomic Structure of Internal Cu/ Al<sub>2</sub>O Interfaces*, *Proceedings Microscopy and Microanalysis 1996*, edited by Bailly, G.W., Corbett, J.M., Dimlich, R. V. W., Michael, J. R., and Zaluzec, N. J., pp 686-687, 1996.
- Gibbesch, B. and Elssner G., *Utra High Vacuum Diffusion Bonded Nb- Al<sub>2</sub>O<sub>3</sub> and Cu-Al<sub>2</sub>O<sub>3</sub> Joints-The role of Welding Temperature and Sputter Cleaning*, Acta metall. mater., Vol. 40, Suppl., pp. S59-s66, 1992.
- Hansen, Paul Lenvig, Brydson, Rik, and McComb, David W., *p-p-like Transitions at the Silicon L<sub>2,3</sub>-edges of Silicates*, Microsc. Microanal. Microstruct., 3, pp. 213-219, 1992.
- Hansen, P L, Brydson, R, McComb, D.W. and Richardson, I., *EELS Finger Print of Al-Coordination in Silicates*, Microsc. Microanal. Microstruct., 5, pp. 173-182, 1994.
- Holowczak, J. E., Greenhut, V. A., and Shanefield, D. J., *Peel adhesion Bond Strength of Direct Bonded Copper-Alumina, Metal-Ceramic Joining*, Edited by Kumar, P. and Greenhut, V. A., The Minerals, Metals & Materials Society, 1991.
- Kaneko, K., ICORP JST, c/o JFCC, Atsuta, Nagoya 456, Japan.
- Kaneko [a], K, Tanaka I., and Yoshiya M, *Six-Fold Coordinated Silicon at Grain Boundaries in Sintered  $\alpha$ -Al<sub>2</sub>O<sub>3</sub>*, Appl. Phys. Lett., 72[2], 1998.



Kaneko [b], K., Gemming T., Tanaka I., and Müllejans H., *Analytical Investigations of Random Grain Boundaries of Zr-Doped Sintered  $\alpha$ -Al<sub>2</sub>O<sub>3</sub> by Transmission Electron Microscopy and Scanning Transmission Electron Microscopy*, Philosophical Magazine A, Vol. 77, No. 5, pp. 1255-1272, 1998

Kingery W. D., Bowen, H. K. and Uhlmann, D. R., *Introduction to Ceramics, 2nd edition*, Wiley, New York, 1976.

Kleebe, Hans-Joachim, Hilz, Gabriela and Ziegler, Günter, *Transmission Electron Microscopy and Electron Energy-Loss Spectroscopy Characterization of Glass Phase in Sol-Gel-Derived Mullite*, J. Am Ceram Soc., 79 [10] pp. 2592-600, 1996.

Leepman, R. D. and Hunt J. A., *Comparison of Detection Limits for EELS and EDXS*, Microsc. Microanal. Microstruc, 2, pp.231-244, 1991.

Müllejans, H. and Bruley, J., *Improvements in Detection Sensitivity by Spatial Difference Electron Energy-Loss Spectroscopy at Interfaces in Ceramics*, Ultramicroscopy, 53 pp. 351-360, 1994.

Müllejans, H. and Bruley, J., *Electron Energy-Loss Near-Edge Structure of internal Interfaces by Spatial Difference Spectroscopy*, Journal of Microscopy, Vol. 180, Pt. 1, October, pp. 12-21, 1995.

Menon, S.K. and Krishnan, K.M., *Charge Transfer and Short-Range Order Cu-Pd and Ni-Mo Alloys*, Philosophical Magazine Letters, Vol. 66, No. 5, pp 271-275, 1992.

Roger, K. A., Trumble, K. P., Dalgeish, B. J., and Reimanis, I. E., *Role of Oxygen in Microstructure Development at Solid-State Diffusion -Bonded Cu/ $\alpha$ -Al<sub>2</sub>O<sub>3</sub> Interfaces*, J. Am Ceram Soc., 77 [8] pp.2036-42, 1994.

Rühle M., *Structure and Composition of Metal/ Ceramic Interfaces*, Key Engineering Materials, VOL. 116-117, pp. 1-40, 1996.

Scheu, C., Dehem, G., Müllejans, H. and Rühle M., *Electron Energy Loss Spectroscopy at Cu/ Al<sub>2</sub>O<sub>3</sub> And Ti/ Al<sub>2</sub>O<sub>3</sub> Interfaces*, Materials Science Forum, Vol. 207-209, pp. 181-184, 1996.

Simpson, Y. Kouth, Carter, C. B., Morrissey, K.J., Angelini, P., and Bentley, J., *The Identification of Thin Amorphous Films at Grain-boundaries in Al<sub>2</sub>O<sub>3</sub>*, Journal of Materials Science, 21, pp. 2689-2696, 1986.

Susnitzky, David W. and Carter, C. Barry, *Structure of Alumina Grain Boundaries Prepared with and without a Thin Amorphous Intergranular Film*, J. Am Ceram Soc., 73 [8], pp.2485-93, 1990.

Swiatnicki, W., Lartigue-Korinek, S. and Laval, J.Y., *Grain Boundary Structure and Intergainular Segregation in  $Al_2O_3$* , Acta metall. mater. Vol. 43, No. 2, pp. 795-805, 1995.

Tomsia, A. P., *Ceramic/Metal Joining for Structures and Materials*, Journal De Physique IV, Colloque C7, supplément au Journal de Physique III, Vol. 3, 1993.

Tomsia, A. P., Saiz E., Tomsia, A.P., Dalgleish, B. J. and Cannon, R. M., *Wetting and Strength Issues in Ceramic/Metal Bonding*, Proc. 4<sup>th</sup> Japan International SAMPE Symposium, Sep. 25-28, pp. 347-356, 1995.

Trumble, K. P., *Thermodynamic Analysis of Aluminate formation at  $Fe/Al_2O_3$  and  $Cu/Al_2O_3$  Interfaces*, Acta metall. mater. Vol. 40, Suppl., pp.S105-S110, 1992.

Williams, D. B., *Practical Analytical Electron Microscopy in Materials Science*, Verlag Chemie International, 1984.

Williams, D. B. and Carter, C. B., *Transmission Electron microscopy, Spectrometry IV*, Plenum Press, New York, 1996.

Yoshino, Y. and Ohtsu H., *Interface Structure and Bond Strength of Copper-Bonded Alumina Substrates*, J. Am Ceram Soc., 74 [9], pp. 2184-88, 1991.

Yoshino, Y. and Shibata, T., *Structure and Bond Strength of a Copper-alumina Interface*, J. Am Ceramic Soc., 75 [10], pp. 2756-60, 1992.



## INITIAL DISTRIBUTION LIST

1. Defense Technical Information Center.....2  
8725 John J. Kingman Rd., STE 0944  
Ft. Belvoir, Virginia 22060-6218
  
2. Dudley Knox Library .....2  
Naval Postgraduate School  
411 Dyer Rd.  
Monterey, California 93943-5100
  
3. Naval/Mechanical Engineering, Code 34 ..... 1  
Naval Postgraduate School  
700 Dyer Rd., Bldg. 245  
Monterey, California 93943-5100
  
4. Department Chairman, Code ME/Mc..... 1  
Department of Mechanical Engineering  
Naval Postgraduate School  
700 Dyer Rd., Bldg. 245  
Monterey, California 93943-5100
  
5. Dr. Alan G. Fox, Code ME/FX .....6  
Department of Mechanical Engineering  
Naval Postgraduate School  
700 Dyer Rd., Bldg. 245  
Monterey, California 93943-5100
  
6. Dr. Sarath Menon, Code ME/MS ..... 1  
Department of Mechanical Engineering  
Naval Postgraduate School  
700 Dyer Rd., Bldg. 245  
Monterey, California 93943-5100
  
7. Richard Y. Hashimoto .....2  
805 Guildford Ave.  
San Mateo, California 94402